# TANK WASTE TRANSPORT STABILITY: SUMMARY OF SLURRY AND SALT-SOLUTION STUDIES FOR FY 2001

**June 2002**

# TANK WASTE TRANSPORT STABILITY: SUMMARY OF SLURRY AND SALT-SOLUTION STUDIES FOR FY 2001

*Compiled by*

**Timothy D. Welch**
Nuclear Science and Technology Division
Oak Ridge National Laboratory

Published: June 2002

# CONTRIBUTORS

**Hani Al Habbash**, Diagnostic Instrumentation and Analysis Laboratory, Mississippi State University, Starkville, Mississippi

**Elizabeth Allan**, AEA Technology, Oxfordshire, UK

**Tushar Durve**, Diagnostic Instrumentation and Analysis Laboratory, Mississippi State University, Starkville, Mississippi

**Anthony Francis**, AEA Technology, Oxfordshire, UK

**Jim Henshaw**, AEA Technology, Oxfordshire, UK

**Rodney D. Hunt**, Nuclear Science and Technology Division, Oak Ridge National Laboratory, Oak Ridge, Tennessee

**James R. Jewett**, Numatec Hanford Corporation, Richland, Washington

**Jeff S. Lindner**, Diagnostic Instrumentation and Analysis Laboratory, Mississippi State University, Starkville, Mississippi

**Ruben D. López**, Hemispheric Center for Environmental Technology, Florida International University, Miami, Florida

**Paul Smith**, AEA Technology, Oxfordshire, UK

**Rajiv Srivastiva**, Hemispheric Center for Environmental Technology, Florida International University, Miami, Florida

**Vijay Raju**, Diagnostic Instrumentation and Analysis Laboratory, Mississippi State University, Starkville, Mississippi

**Steven Swanton**, AEA Technology, Oxfordshire, UK

**Rebeca K. Toghiani**, Department of Chemical Engineering, Mississippi State University, Starkville, Mississippi

**Timothy D. Welch**, Nuclear Science and Technology Division, Oak Ridge National Laboratory, Oak Ridge, Tennessee

# CONTENTS

## PREFACE

This report provides, in one convenient document summary, articles on studies of tank waste slurry transport and salt-well pumping at the U.S. Department of Energy's Hanford site in southeastern Washington state. These studies were performed in FY 2001 by five different organizations. The studies are concerned with the chemistry and stability (steady, uninterrupted flow) of tank waste transfers as a collaboration among AEA Technology, the Diagnostic Instrumentation and Analysis Laboratory at Mississippi State University, the Hemispheric Center for Environmental Technology at Florida International University, the Numatec Hanford Corporation, and the Oak Ridge National Laboratory.

The document has been lightly edited for a consistent format, but much of the original flavor (technical content and style) of each institution's contribution has been retained. Readers are encouraged to consult the individual detailed reports published by each of the contributors or to contact the authors for more detailed information.

During the course of the work, researchers provided current results to site engineering organizations, and the latter provided real-time feedback through regular biweekly conference calls and annual on-site workshops.

# 1. INTRODUCTION

Despite over 50 years of experience in transporting radioactive tank wastes to and from equipment and tanks at the Department of Energy's Hanford, Savannah River, and Oak Ridge sites, waste slurry transfer pipelines and process piping become plugged on occasion. At Hanford, several tank farm pipelines are no longer in service because of plugs. At Savannah River, solid deposits in the outlet line of the 2H evaporator have resulted in an unplanned extended downtime. Although waste transfer criteria and guidelines intended to prevent pipeline plugging are in place, they are not always adequate. To avoid pipeline plugging in the future, other factors that are not currently embodied in the transfer criteria may need to be considered. The work summarized here is being conducted to develop a better understanding of the chemical and waste flow dynamics during waste transfer. The goal is to eliminate pipeline plugs by improving analysis and engineering tools in the field that incorporate this understanding.

Predictive models for pipeline transport of tank wastes are needed to provide a solid basis for transport system design and operation and for development of reliable program schedules. Such models are important because they enable "what-if" studies, permitting plans to be made well ahead of time. This advance planning lowers construction costs and minimizes process upsets. Slurry flow tests are an essential part of the pipeline flow models. They provide the input data to develop correlations and provide feedback to check established correlations.

Information about agglomeration in wastes is important because of the effect that agglomerates have on viscosity, solids settling rates, and other waste characteristics that affect pumping. The rates of formation and break-up of agglomerates and the durability of agglomerates under turbulent conditions in pumps and in pipeline flow are all important characteristics that feed into the transport prediction models.

The emphasis of the work reported here is on tank waste dynamics during transport. The static and equilibrium aspects of tank waste chemistry, including solubility studies, chemical phase equilibrium, solids identification and waste viscosity, have been described by Hunt et al. (2002), Herting (2001), and Toghiani et al. (2002). The first article discusses some of the predictive models currently being used to analyze tank waste transport, identifies potential plugging mechanisms that may be encountered, and lists some of the limitations of current models. It describes the modeling capabilities and data requirements to analyze waste transfers for the variety of plugging mechanisms that may be encountered. Experimental studies are being conducted utilizing simulated wastes. The second article describes the development of simulated tank waste (AY-102 and AZ-101) recipes by Oak Ridge National Laboratory for use by collaborators at Florida International University (FIU). In the third article, AEA Technology describes results from its literature review on particle agglomeration and provides a preview of work to measure agglomeration and breakup rates on simulated sludge relevant to Hanford wastes.

Slurry flow tests are essential to validate the pipeline flow models to check established correlations. The fourth article describes the FIU studies related to cross-site slurry transfers with phosphate-fluoride solutions and simulated tank AY-102 and AZ-101 wastes to measure pressure drops, plugging dynamics, slurry rheology, and particle characteristics. Fluid flow rates, pipeline diameter, waste composition, temperature reduction, and waste solid volume fraction were studied by FIU in several pipe loops to evaluate the plugging potential of simulated Hanford wastes and to help determine the operating boundary conditions for stable waste transfer.

Cross-site transfers are carried out in the turbulent flow regime. The pumping of salt solution from salt wells, on the other hand, is in the laminar flow regime. The salt solutions may be saturated and may become supersaturated if the solution is cooled during the transfer, and salt-well pumping lines have plugged occasionally as a result. In the fifth article, researchers at the Diagnostic Instrumentation and

Analysis Laboratory at Mississippi State University (MSU) describe tests with simulated SX-104 waste in a flow loop to simulate salt-well pumping and related Environmental Simulation Program equilibrium calculations.

Initial work at MSU to explore computational fluid dynamics modeling of tank waste transfers and "computational experiments" to test engineering correlations currently in use will be published in a separate document.

Results from FY 2001 studies include the following:

- Six distinct pipeline plugging mechanisms were identified, and the situations are identified where mechanisms other than the baseline need to be considered.
- The best plugging prevention or recovery strategy depends on the specific formation mechanism and chemical system.
- Waste simulants were formulated for tanks AY-102 and AZ-101.
- Plug-free transfer of Hanford AZ-101 and AY-102 simulated waste was demonstrated in a pilot-scale pipe test loop, even under the worst credible flow and environmental conditions.
- The simulated AZ-101 and AY-102 wastes showed a non-Newtonian Bingham plastic rheological behavior.
- The mean particle size of 100-200 µm is consistent with the measurements reported by Jewett and Jensen (2000) for Hanford sludges.
- Particle growth rates, agglomeration rates, and time-to-plug were measured for salt solutions in a flow test loop to evaluate salt transfer operations.
- The theory of agglomeration, de-agglomeration, and particle settling and re-suspension has been reviewed. At the high ionic strengths in the waste tanks, agglomeration is inevitable.
- The important factors contributing to the rate of agglomeration and final size of the agglomerate are the primary particle properties and the turbulent energy density dissipation rate.
- The experiments that are currently in progress on the system comprising gibbsite, boehmite, $Fe(OH)_3$, and $SiO_2$—a simple representation of the sludges contained in the Hanford tanks C-103 and C-104—are also described here.

## 1.1 References

Herting, D. L., 2001. *Saltcake Dissolution FY 2001 Status Report*, HNF-8849, Rev. 0, Fluor Daniel Hanford, Richland, Washington, (September).

Hunt, R. D., J. S. Lindner, A. J. Mattus, J. C. Schryver, and C. F. Weber 2002. *Waste Preparation and Transport Chemistry: Results of the FY 2001 Studies*, ORNL/TM-2001/289, Oak Ridge National Laboratory (February).

Jewett, J. R., and L. Jensen. 2000. *Assessment of Available Particle Size Data to Support an Analysis of the Waste Feed Delivery System Transfer System*, RPP-6247, CH2MHill Hanford Group, Inc., Richland, Washington (August).

Toghiani, R. K., and J. S. Lindner 2002. *DIAL/MSU Saltcake Dissolution Project, FY '01 Status Report,* DIAL TR01-1 Tank Focus, Diagnostic Instrumentation and Analysis Laboratory, Mississippi State University, Starkville, Mississippi (in preparation).

<div align="right">

James R. Jewett
Timothy D. Welch

</div>

# 2. TANK WASTE TRANSPORT, PIPELINE PLUGGING, AND THE PROSPECTS FOR REDUCING THE RISK OF WASTE TRANSFERS[*]

Timothy D. Welch

Oak Ridge National Laboratory

## Abstract

This report evaluates some of the modeling tools currently being used to analyze waste transfers at the U.S. Department of Energy's Hanford site. The additional modeling capabilities and data needed to address the limitations of the current tools are identified, and approaches to implementing these new capabilities are described. Application of improved waste transfer models will result in greater confidence in predictions of waste behavior under both normal and upset transfer conditions.

Six distinct waste-pipeline–plugging mechanisms are identified. However, the tools currently being used by the site for design and waste transfer evaluations can directly address only one of these, solids settling from a slurry with a static particle-size distribution (PSD) to form a plug. The five additional plugging mechanisms are as follows:
- settling of solids having a dynamic PSD (as a result of chemical reactions, reaction, precipitation, agglomeration, fragmentation, etc.);
- surface deposition of solids (for static or dynamic PSD) due to adhesion, deposition, or crystal nucleation at the surface;
- bulk or slug plugging, where the entire cross section becomes blocked very rapidly;
- formation of a packed bed at the foot of a vertical pipe leg; and
- solids settling and deposition at dead-flow zones near elbows, flow constrictions, etc.

The current waste transfer analysis does not directly consider precipitation, gelation, chemical reaction kinetics, particle agglomeration, particle breakup, and other dynamic processes that occur in some sludge and salt waste transfers. Nor do the current methods account for waste-surface interactions or the coupling of waste chemistry and flow (i.e., how chemistry affects the flow, and how flow affects the chemistry). Accounting for some of these dynamic processes is needed to predict four of the six identified plugging mechanisms.

Development of improved waste transport modeling tools with improved capabilities is needed to evaluate completely and accurately the plugging risk of some waste transfers. Approaches to developing these capabilities are outlined in the report. Such capabilities will also help the site assess cost-reduction strategies, develop process control strategies, design transfer piping, and diagnose plugging events. Accounting for PSD dynamics along the flow route will be pursued first to provide some of the capabilities needed to evaluate several additional plugging mechanisms. Transport model development work in FY 2002 will focus on (1) salt solution transport projects and operations and (2) improvements to the hindered settling correlation to account for settling of polydispersed solids and particle shape in slurry transport.

---

[*]This section is condensed from the report with the same title, ORNL/TM-2001/157 (August 2001). Please see the full report for details.

## 2.1 Introduction

At the U.S. Department of Energy Hanford Site, 55 million gallons of radioactive wastes is stored in 177 underground storage tanks (149 single-shell tanks and 28 double-shell tanks). The wastes in the tanks include insoluble sludge, saltcake precipitated from salt solutions, and liquid supernatant, that are typically salt solutions. To treat this waste and put it in a form suitable for final disposition, the waste must be retrieved from the tanks and either transported to other tanks for interim storage or waste staging, or transferred directly to a waste treatment facility. Several types of transfers take place:

- pumping of supernatant liquids from above the layer of settled solids (decanting);
- pumping of interstitial liquid from the pore spaces in the saltcake layer ("salt-well pumping," also referred to as "interim stabilization");
- pumping salt solution that results from the dissolution of the saltcake; and
- pumping of sludge-water, sludge-supernatant, and sludge-salt-supernatant slurries.

Plugging of waste transfer pipelines has occurred occasionally during waste transfers of both salt solutions and sludge slurries. This plugging has been attributed to a variety of causes:

- settling of solids because the flow rate was too low or the solids volume fraction was too high;
- operational upsets—interruption of the waste flow, inadvertent entrainment of solids in the feed, and changes in environmental temperature;
- chemical instability—precipitation, gel formation, or other transformations due to temperature changes, local concentration changes, or mixing and pumping of several wastes that are not in equilibrium;
- hydrodynamic instability—transition of the flow from one flow regime to another (turbulent to laminar) or from one flow pattern to another (homogeneous to heterogeneous) as a result of an external change or as a result of changes in slurry properties occurring during transit;
- piping components that are prone to solids deposition—sharp bends such as those found in Hanford PUREX connectors, unheated jumpers, flow restriction, etc.;
- deposition of solids; and
- crystal growth on surfaces.

At Hanford, the Environmental Simulation Program™ (ESP) is sometimes used to estimate the initial composition and the solids content of the waste salt solution prior to transfers.

Semiempirical fluid mechanics correlations are used to calculate flow velocities and pressure drops for waste slurry transfers. These tools are used in tandem to evaluate waste transfers, plan for waste feed preparation and delivery, and design piping systems.

The exact location of the operating envelope boundary that defines a stable waste transfer for a particular waste is uncertain. Site waste transport criteria, the working definition of the operating envelope, have been developed based primarily on fluid dynamics considerations. But uncertainties in the operating envelope boundary come from several sources: waste characterization data, fluid dynamics behavior, chemical dynamics, properties, and limitations in our model's ability to describe these phenomena accurately.

## 2.2 Primary Current Tank Waste Transport Analysis Tools

### 2.2.1 Waste Slurry Transport Analysis at Hanford

Hanford waste transfer criteria limit the slurry solids content to less than 30 vol% and require a Reynolds number (Re) of greater than 20,000 (Estey and Hu 1998) to remain within the piping pressure rating and to prevent solids from settling in the transfer line. In practice, a minimum average velocity of 6 ft/s and a maximum specific gravity (1.41) are used. These criteria assume that the solids in the slurry do not change during the transfer (i.e., that they are static), are based on steady-state fluid flow, and do not consider the consequences of chemical processes such as precipitation. If solids are formed during the transfer as a result of chemical processes, the volume percent of solids increases and the Re value decreases, possibly moving outside the criteria limits.

Recent pipeline hydrodynamic analyses at Hanford (Julyk, Oten, and Willis 2000) have used the correlation of Oroskar and Turian (1980):

$$v_c = 1.85 \sqrt{gd(s-1)}\, C^{0.1536} (1-C)^{0.3564} \left(\frac{d}{D}\right)^{-0.378} \overline{N}_{Re}^{0.09}\, x^{0.30} \quad . \tag{1}$$

This equation is written in terms of the particle diameter ($d$), pipe diameter ($D$), solid and liquid density ($\rho_l$) solids volume fraction ($C$), modified Re ($\overline{N}_{Re}$), viscosity of the liquid ($\mu$), and fraction of eddies with velocities exceeding the hindered settling velocity of the particles ($x$). The form of the equation was patterned after a semiempirical equation derived by making a number of limiting assumptions. Most of the properties in the equation are relatively easily measurable, except for $x$. This parameter depends on the hindered settling velocity of the particle. Analyses have used expressions for hindered settling derived from Richardson and Zaki (1954) for monodispersed spherical particles. The Richardson and Zaki equation is not accurate for polydispersed and nonspherical particles.

The Oroskar and Turian correlation is applicable to the flow of heterogeneous slurries of single-sized spherical particles. The physical properties, transport properties, particle-size distribution (PSD), and temperature are assumed to be the same for the entire length of the pipeline. No information is provided about the local velocity profile, the local solid bed depth, the local liquid concentration, the solids volume fraction, the solids PSD, the temperature, etc., along the length of the pipe. Nor does this correlation describe how these quantities change with time.

The following discussion summarizes some of the limitations of the critical velocity correlation of Oroskar and Turian—which have been identified in previous reviews (Liddell and Burnett 2000; Estey and Hu 1998)—as well as a few additional issues.

**Extrapolating beyond the range of the original mean particle size and PSD data.** Liddell and Burnett (2000) have recently published a comprehensive literature review for the Hanford River Protection Project (RPP) on critical transport velocity correlations and models. The review indicates that most of the experimental data upon which these correlations are based were obtained for heterogeneous slurries with solids having relatively large (150-µm), but narrowly graded, particle size. On the other hand, the Hanford tank solids that have been examined (Jewett and Jensen 2000) appear to have a broad PSD with a mean particle size of 110 µm and a substantial fraction of particles of less than 100 µm. This suggests that the tank waste be modeled as settling flow (the large particles) with a homogeneous carrier fluid (the carrier liquid plus the fine particles). Since both the mean particle size and the PSD of the tank wastes are different from those of the slurries used to derive the correlations in the literature, application of these to tank wastes is an extrapolation. Liddell and Burnett (2000) conclude that ". . . there is no published

empirical critical velocity equation that is directly applicable to Hanford tank waste slurries." The existing correlations, with the exception of that of Gillies and Shook (1991), were regressed from data for slurries with narrow size distributions and a mean particle size of 100 μm or larger. Jewett and Jensen's (2000) analysis of the best available data for Hanford tanks indicated a broad PSD with a significant fraction of particle sizes below 100 μm. Liddel and Burnett recommended that the correlations be validated by experimental work.

**Hindered settling.** Oroskar and Turian (1980) explicitly account for hindered settling in their correlation by incorporating the relationship described by Maude and Whitmore (1958), which is similar to the Richardson and Zaki equation (1954). However, this equation fails for polydispersed and nonspherical particles. In accounting for hindered settling, a strongly nonlinear function of solids volume fraction, PSD, and particle shape is essential for accurate predictions in all but the most dilute slurries. Work is ongoing at Florida International university (FIU) to obtain experimental data to check the correlation.

**Slurry viscosity.** The viscosity depends on volume percent solids, particle size, PSD, and particle shape. Slurry viscosity data and viscosity models that account for these factors are needed for homogeneous slurries. The carrier fluid viscosity and the particle settling velocity must either be measured for the specific conditions under consideration or estimated by a model.

**Static PSD.** The critical velocity correlations that have been considered assume that the PSD is static; that is, it does not change in transit. For some types of wastes, such as sludges and salt slurries, the PSD changes during transfer as a result of precipitation, particle breakup, particle agglomeration, settling, or interactions with surfaces. Pipeline plugging is fundamentally a transient process in one-, two-, or three-dimensional space, depending on the particular plugging mechanism. For slurries with dynamic PSDs, the Oroskar and Turian correlations might still be used for predicting the critical velocity if the particle dynamics are slow [Damköhler number (Da) $<<$ 1] or very fast (Da $>>$ 1) relative to the transport times. (The Damköhler number used here is the ratio of the characteristic flow time to the chemical reaction time: Da $= t_{flow}/t_{chem.rxn}$.) If the purpose of the analysis includes dynamic process control, investigation of plug formation, or evaluation of unplugging methods, then the transient case must be considered as well.

### 2.2.2 Computational Fluid Dynamics Modeling of Waste Slurry Transport

Use of computational fluid dynamics (CFD) for waste transport modeling is at the opposite end of the spectrum of rigorous physics and complexity from the simpler, empirical approach based on bulk constant properties discussed previously. In the CFD approach, the Navier-Stokes equations are solved numerically to compute the velocity, distribution, and pressure profile of the slurries over the pipeline space and the duration of the transfer. In addition, the local particle concentration, PSD, solids deposition, and physical and transport properties can be computed by incorporating kinetic models for chemical reactions, precipitation, agglomeration, and other processes. The possibilities of this approach include a case-by-case description detailed in space and time of the slurry flow, plug formation, and unplugging. But simplifications are still required for this approach to be practical. The goal was to be able to define and run a case in a few days, using computers that would be available to design and analysis staff. The challenge is to identify those simplifying assumptions that will permit practical solutions to real problems while still capturing the essential physics and chemistry. [See Kuipers and van Swaaij (1998) for a review of the state of the art of CFD in chemical engineering.]

CFD has the potential to provide the relevant engineers (design, field, and control) with important new capabilities, such as axial velocity, pressure, and settled bed profiles. When coupled with kinetics of precipitation, agglomeration, and fragmentation, CFD may also be useful for predicting local solids concentration, PSD, and transient pressure and flow signatures.

6

However, the implementation of CFD modeling also has limitations:

- Constructing the computational mesh for complicated pipe geometries may be time-consuming.
- The time to run individual cases can be many days on a Pentium III dual-processor workstation.

Some outstanding issues with the application of CFD to slurry transport include the following:

- The accuracy of the approximations used for solid-liquid flow, especially for concentrated (>0.1% solids) slurries, remains problematic. For dense suspensions, four-way coupling is present; that is, the fluid flow affects particle motion, the particle motion affects fluid structure, and particles interact with other particles (e.g., Levenspiel 1962).
- Describing the physics of the settled bed dynamics is very difficult; thus, simplifying assumptions must still be made in applying CFD.
- The chemical kinetics that are included must be relatively simple so that problems can be solved in a reasonable time.

For these reasons, the work on CFD to support immediate site waste transport needs is being de-emphasized by the Tanks Focus Area (TFA) in FY 2002. CFD will eventually play a role in the analyst's tool kit for specialized applications, as CFD becomes easier to implement, faster computers become available to the design and analysis staff, and theoretical difficulties are overcome. In Sect. 4, a model development approach is proposed that addresses some of these difficulties and lays the groundwork for future CFD implementation.

### 2.2.3 Modeling of Salt Solution Transport

The RPP and the TFA have done a great amount of work over the last few years to validate and enhance ESP, a computer code that models the equilibrium chemistry of electrolyte solutions. ESP predicts the liquid-phase composition, the solid phases that are formed, and the quantity of solids formed for an input composition. The ESP code has been used for a number of applications at Hanford. These applications include estimating the compositions and phases of waste mixtures for feed preparation, estimating the dilution water required for dissolving saltcakes, and estimating the dilution required for salt-well pumping.

Salt solution may be pumped from tank salt wells, from saltcake dissolution operations, or as a suspension for transporting sludge. The solution may be nearly saturated, and, in many cases, the flow is in the laminar regime. ESP is used to estimate how much dilution water must be added so that the solids content is low enough to meet waste transfer criteria. If the salt solution has few solids (<0.1%), the solution is typically considered to be a liquid for purposes of hydraulic analysis, and standard methods for liquids are then applied. The maximum quantity and the types of solids that may form because of cooling during transport or other process upsets may also be calculated by a chemical equilibrium code such as ESP prior to a transfer.

### 2.3 Plugging Mechanisms and the Coupling of Chemistry and Fluid Dynamics

Hanford's waste transfer criteria are based primarily on fluid dynamics considerations. The volume fraction of solids is limited to 30 vol% so that the slurry viscosity and the pressure required to pump the slurry do not become too high. A minimum velocity is specified to keep slurry solids suspended during transfer. ESP is sometimes used to predict the initial solids fraction of solids and slurry properties. The criteria are designed to provide a slurry that is pumpable and stable with respect to settling. But settling is

only one of several plugging mechanisms that have been observed, suspected, or postulated based on assessments of plugging events.

To adequately assess the stability of a waste transfer, all of the credible plugging mechanisms for that transfer must be evaluated. Most sludge-water transfers could probably be safely accomplished by operating within the fluid dynamics–based transfer criteria, but operating experience suggests that the same is not true for all waste transfers. It is desirable to identify these potentially problematic waste transfers in advance so that stable transfer conditions can be specified.

### 2.3.1 Pipeline Plugging Mechanisms

Pipeline plugs may form via a variety of mechanisms. Some of the mechanisms that have been observed or postulated for tank waste transfers are illustrated in Table 1. These plugging mechanisms are summarized in Fig. 1 and are described in this section.

**Table 1. Tank waste plugging mechanisms in pipelines**

| Plugging mechanism | Description of plugging mechanism | Where mechanism has been observed or suspected or could exist | Limiting conditions |
|---|---|---|---|
| 1. Solids settling, static PSD (see Fig. 1a) | Solids settle on the bottom of the pipe from a slurry with a static PSD | Cross-site transfers of sludge-water slurry | Flow velocity, solids volume fraction, solids density, solids PSD, temperature |
| 2. Solids settling, dynamic PSD (see Fig. 1b) | Solids settle on the bottom of the pipe from slurry with a dynamic PSD due to precipitation, agglomeration, etc. | Cross-site transfer or sludge-supernatant slurry and salt-well pumping (salt solution) | Flow velocity, solids volume fraction, solids density, solids PSD, precipitation rates, chemical reaction rates, agglomeration rates, temperature |
| 3. Surface deposition and crystallization (see Fig. 1c) | Solids adhere to the pipe surface or crystallize on the surface | Evaporator lines of Savannah River. Solutions containing silica and alumina | Surface deposition rates, crystallization rates, flow velocity, temperature |
| 4. Bulk or slug plugging | Flow keeps rapidly-forming solids suspended until entire cross section is plugged | Salt solutions containing phosphate | Flow velocity, flow regime, metastable state formation kinetics, temperature |
| 5. Packed bed in vertical flow | Packed bed forms at the base of vertical leg if flow rate is below the terminal velocity | Vertical legs leading to Waste Treatment Plant | Flow velocity, solids volume fraction, PSD, solids density, temperature |
| 6. Depositions at elbows, constrictions, etc. | Solids deposit at low-flow zones | PUREX connectors. Orifices in valve pits | 3-D velocity field, flow velocity, solids volume fraction, solids density, solids PSD, precipitation rates, chemical reaction rates, agglomeration rates, temperature |

PSD = particle size distribution.
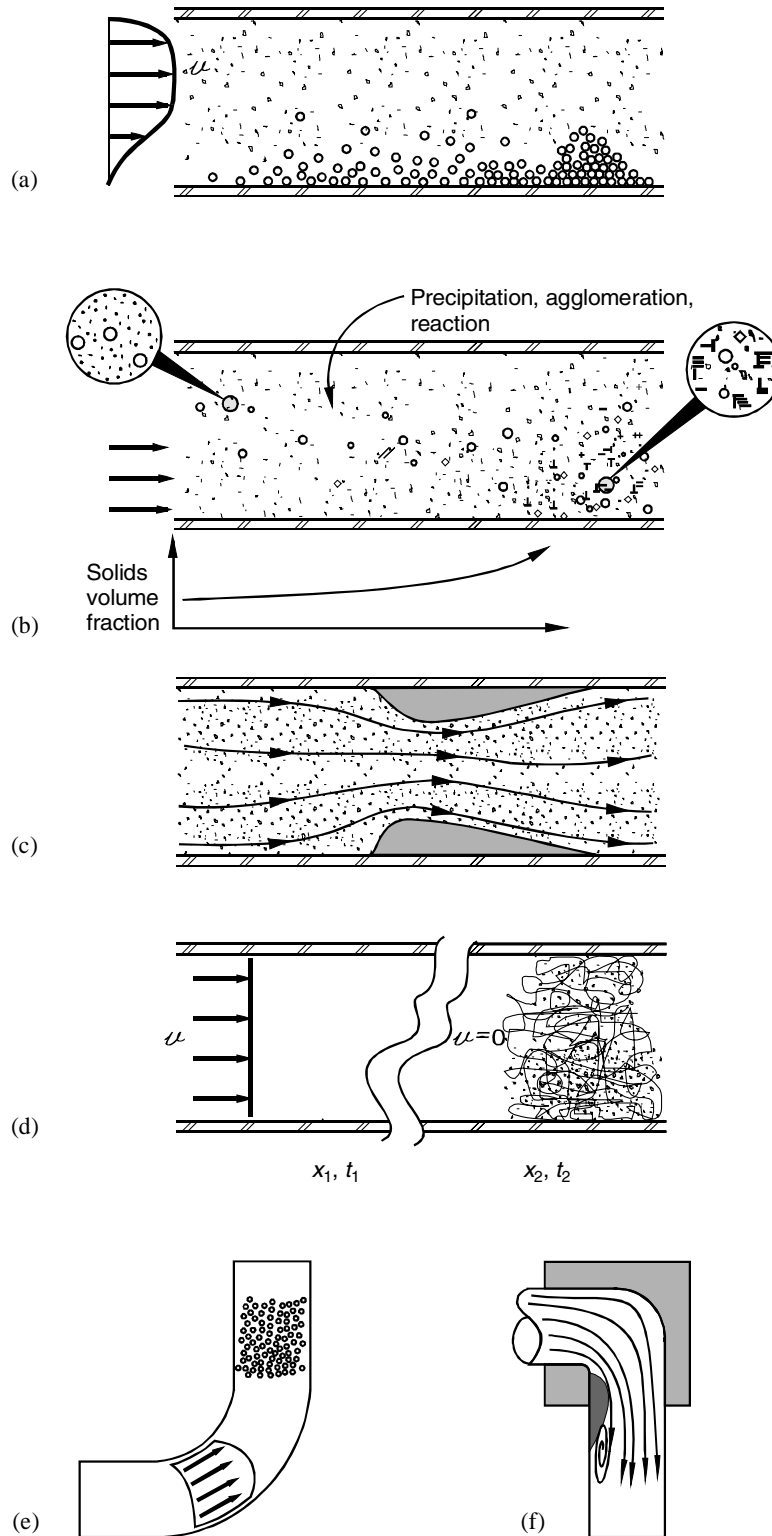3D = three-dimensional.

8

**Fig. 1. Waste pipeline plugging mechanisms.** (a) Solids settling (static particle-size distribution), (b) solids settling (dynamic particle-size distribution), (c) surface deposition, (d) bulk or slug plugging, (e) packed bed formation in vertical leg, and (f) deposition at flow "dead zones" in elbows.

**Mechanism #1: Solids settling (slurries with a static PSD).** Much of the waste transfer analysis at Hanford has focused on this mechanism of pipeline plugging. Solids from the waste slurry settle because the flow velocity is insufficient to keep them suspended. The settled solids form a stationary bed that eventually fills the pipe and blocks flow. The critical velocity and pressure drop are calculated based on the slurry's physical and transport properties, as well as the pipe dimensions. These critical velocity correlations can also be used in some cases for dynamic PSDs: that is, if the particle dynamics are slow (Da << 1) or very fast (Da >> 1) relative to the transport times.

**Mechanism #2: Slurry flow with dynamic PSDs due to particle agglomeration, fragmentation, precipitation, or chemical reaction.** In actual waste transfers, the slurry PSD is frequently dynamic. The shear stress of the pump or of the turbulent flow may break up fragile agglomerated particles. Chemical adjustments, mixing of waste streams, or particle-particle interactions during transport may promote particle agglomeration, resulting in larger particles. Cooling of the slurry in transit or fluctuations in local concentrations may initiate crystallization from the liquid carrier and result in a higher solids volume in the slurry. If the kinetics of these processes are very slow relative to the transfer residence time, then the critical velocity and pressure drop can be calculated based on the initial slurry properties; but analysis of solids deposition on pipe walls and similar phenomena would still need to consider the slow solids formation kinetics. If the kinetics of these processes are very fast, then the critical velocity and pressure drop can be calculated based on the final slurry properties, provided that there are not "catastrophic" changes in the slurry properties (see mechanism 4). However, if the kinetics of the process are on the same order of magnitude as the transfer residence time (Da ≈ 1), the PSD dynamics along the flow path may need to be included, depending on the objectives of the analysis. Analysis of this mechanism requires that models account for both flow phenomena and particle dynamics. This mechanism could apply to salt-well pumping or some waste slurry transfers.

**Mechanism #3: Uniform deposition of solids on pipe wall and other surfaces.** If solids attach to the pipe wall, a solid layer could build up that would eventually choke off flow. Some components in the waste may adhere to the wall, or the wall could serve as a nucleation site for crystallization. The roughness of the wall and material of construction would influence which compounds adhere. Uniform growth of a deposition layer is more likely to occur in the laminar flow regime but could also occur in turbulent flow. Analysis of this mechanism requires that models account for both flow phenomena and particle dynamics. This mechanism could apply to salt or sludge transfers. Deposits that appear to have been formed by this mechanism have been observed in evaporator piping at Savannah River. See Hu et al. (2001) for results of recent tests aimed at understanding scale formation in the 2H evaporator.

**Mechanism #4: Bulk "instantaneous" plugging.** Rapid reactions—such as that associated with the change in the waters of hydration of phosphates and formation of metastable colloidal phases and gels—could account for a slurry's remaining a pumpable fluid until a local critical condition is reached, resulting in a very rapid transition. The result is a nearly instantaneous dramatic change in the local property, such as the viscosity, particle volume fraction, PSD, or morphology. This mechanism could be modeled by relatively simple treatment of the fluid velocity profiles, but it would require a good description of the chemical kinetics and other phenomena that control the bulk plug formation. See Hunt et al. (2000) for examples of both sludge and salt solutions that could be susceptible to this bulk plugging behavior

**Mechanism #5: Upward flow in vertical pipes.** In vertical pipe runs, the liquid velocity must exceed the terminal velocity of the largest particle in the slurry. A bed of solids will form at the base of the vertical leg if the velocity is too low. This mechanism of plugging can occur with salt and sludge transfers.

**Mechanism #6: Solids deposition at elbows, constrictions, and other flow dead zones.** Solids may deposit at a sharp elbow due to the impingement and sticking of solid particles onto the wall, or solids

may accumulate in dead zones in the flow system. Since this mechanism involves three-dimensional turbulent flow, predicting this disposition would require the most sophisticated fluid dynamics treatment.

### 2.3.2 The Coupling of Fluid Dynamics and Chemistry

To calculate the critical velocity and the pressure drop for slurries containing narrowly sized, static, spherical particles, the solids volume fraction, particle diameter, particle density, liquid density, and viscosity of the liquid carrier are required. If the solids are polydispersed and nonspherical, then the PSD and particle-shape distribution must also be known. The solids volume fraction, mean particle size, PSD, and particle shape also influence the viscosity of the homogeneous slurry (e.g., Macosko 1994) and the particle hindered settling velocity (e.g., Shor and Watson 1990). The dependence of viscosity and settling velocity on solids volume fraction is strongly nonlinear.

PSD and particle shape directly and indirectly affect the velocity distribution and the settling of particles in the slurry. The baseline correlation presented in Sect. 2.1 does not account for PSD or particle shape and assumes that the mean particle diameter does not change during a transfer.

Fluid dynamic forces and changes in the chemical environment, temperature, and pressure can all result in dramatic changes in the slurry particle properties in transit, which in turn result in dramatic changes in the flow behavior. Some of the chemical and mechanical phenomena that may be encountered are listed below.

- Breakup of solids due to shear forces
- Agglomeration of particles due to changes in the chemical environment, particle-particle interactions, or shear
- Precipitation and chemical reaction
- Ordering and clustering of solids due to the fluid-particle flow field
- Nonequilibrium of flowing systems

Chemistry affects flow and flow affects chemistry (see Fig. 2). When can coupling be ignored and when must it be considered? To address some of these questions, experimental work with simulated sludge wastes and salt wastes is being conducted by the TFA at FIU and Mississippi State University (MSU), respectively. But to interpret and apply these data, models with capabilities beyond those currently in use are required. Models are needed that have enough chemistry and fluid dynamics to describe essential features of waste flow but are simple enough to be developed and deployed to current site problems.

### 2.4 Prospects for Improved Transport Analysis Tools and Risk Reduction

### 2.4.1 Assessment of Existing Tools and Procedures

The existing tools and procedures do not directly address the various plug formation mechanisms or the waste dynamics during transport discussed in the previous section. Limiting the chemistry analysis to equilibrium calculations has several consequences. On the one hand, the predictions may be overly conservative. If a stable species not initially present is predicted from the initial waste composition and planned transfer conditions, but the rate of formation is very slow, then the amount of water or other carrier liquid the prediction calls for will be higher than is actually required. Of course, we would also need to assess the consequences of process upsets and interruptions. On the other hand, the equilibrium chemistry prediction may be too optimistic. The equilibrium calculations yield the final products but provide no information about the concentration of any intermediates formed in transit. The concentration and the in-flow behavior of intermediates cannot necessarily be interpolated from the initial and final
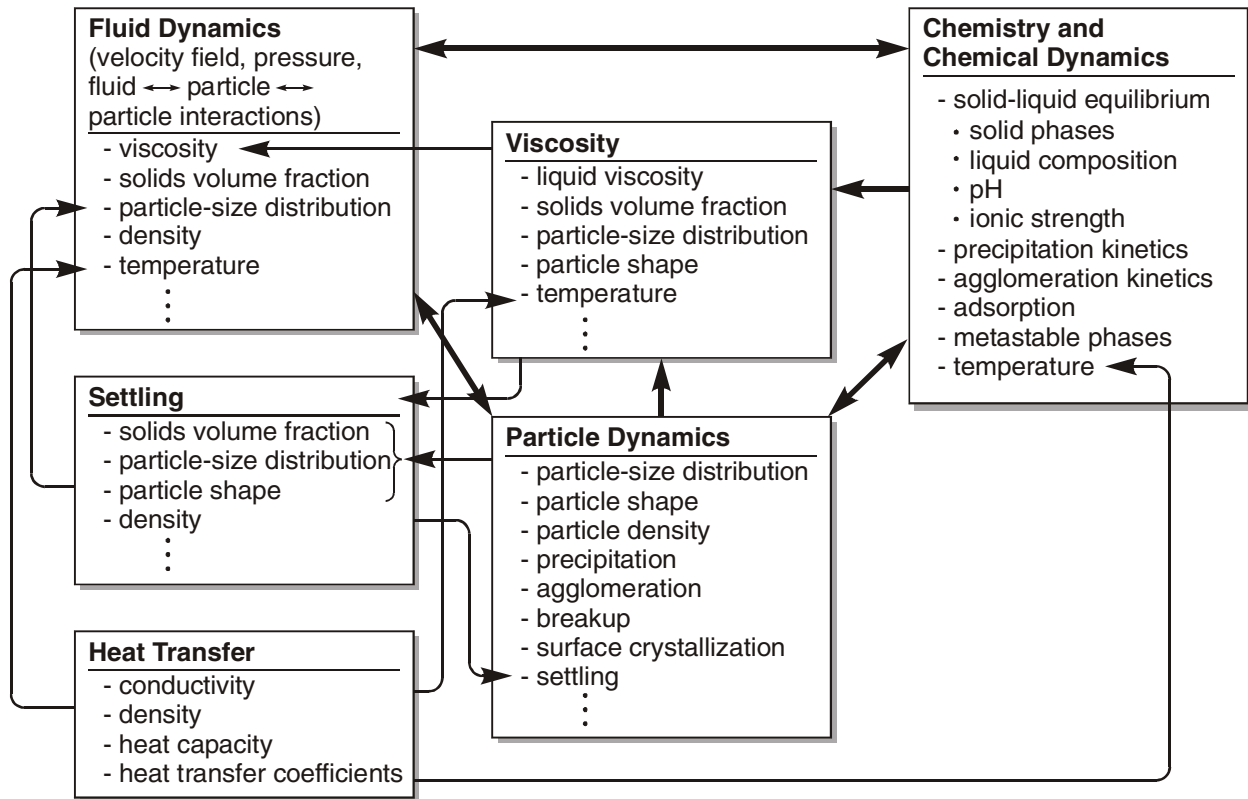
**Fig. 2. Coupling of fluid dynamics and chemistry in waste transport.**

equilibrium states. Nor does the equilibrium calculation predict the formation of gels or metastable phases for which formation is influenced by chemical–flow coupling. The critical velocity slurry flow correlations provide no information about the spatial and dynamic behavior as discussed before.

**2.4.2 Capabilities Needed for Waste Transfer Evaluations**

There are four possible paths to a more complete and accurate description of waste transport behavior and stability (Fig. 3). Path 1 concentrates on describing the fluid dynamics, adding chemical and particle dynamics along the way. Path 2 concentrates on the chemistry, equilibrium, and kinetics and then adds the coupling with flow. Path 3 attempts to account for all aspects at once, a very complex and difficult problem. Path 4 includes key features of both the flow and chemistry, moving incrementally toward a more complete and accurate description of waste transport behavior. This path is proposed here to balance completeness, accuracy, and near-term application. This approach will put practical tools in the hands of site designers and analysts as soon as possible.

Efforts to extend and validate current models being used to evaluate waste transfers are necessary and worthwhile. However, these efforts alone are not sufficient and will neither provide the tools needed to reduce most uncertainties, nor address transfer scenarios beyond the capabilities of current methods of analysis. Furthermore, new modeling capabilities provide the tools for many additional beneficial applications, as outlined in this section. Table 2 outlines the capabilities needed in future tools, their potential application, and the benefits of their use. The choice of predictive tools to evaluate a waste transfer depends on both the purpose of the evaluation and the plugging mechanisms most likely to be relevant for that transfer.
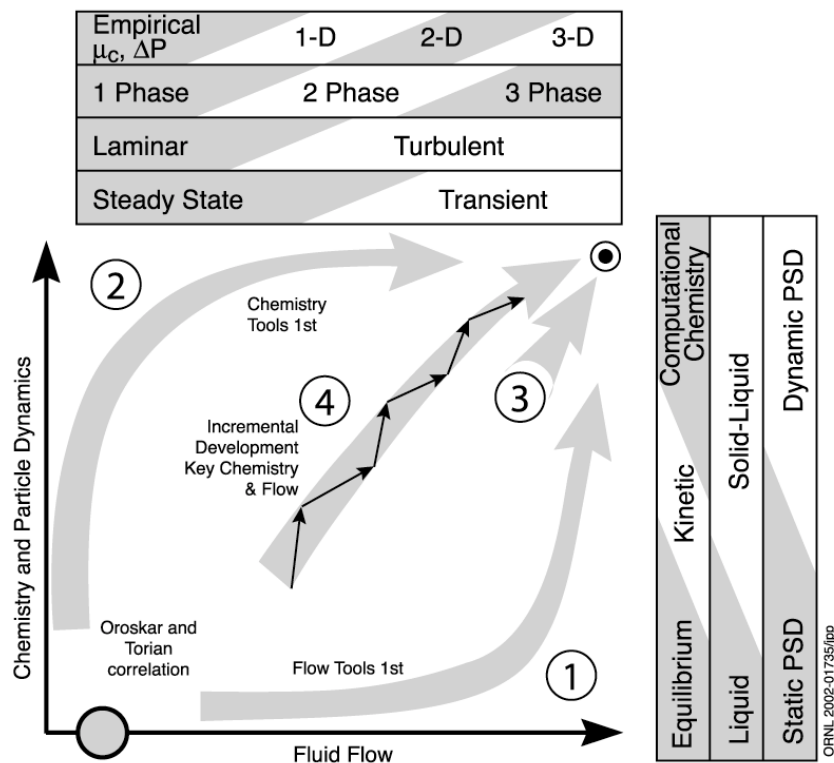
**Fig. 3. Development paths for complete and accurate waste transport analysis.** Path 1—emphasis on fluid dynamics, Path 2—emphasis on chemistry, Path 3—complete accounting of both flow and chemistry, and Path 4—incremental advancement of key flow and chemistry phenomena.

Progress is being made in extending and validating the empirical correlations for slurry flow with a static PSD (mechanism 1). TFA work is ongoing at FIU to obtain data for slurries with solids having a PSD similar to that of the Hanford wastes. These data are then regressed by researchers at FIU and Pacific Northwest National Laboratory to adjust correlation parameters. Under another TFA task at Oak Ridge National Laboratory (ORNL) in FY 2002, viscosity and hindered settling models that account for solids volume fraction, PSD, and particle shape are being reviewed and adapted for applications with these correlations. Measurement of the viscosity of simulated wastes to provide needed data is an ongoing effort at ORNL.

Work to develop the data and data models and to describe the dynamic PSD (mechanism 2, row 2 of Table 2) is also under way. AEA Technology is measuring kinetic constants for precipitation and agglomeration (Henshaw 1999; Francis et al. 2000). In FY 2002, models will be developed to add some of the capabilities listed in Table 2 under "Predictive tools, data, and data models needed" for dynamic PDS (mechanism 2) and bulk plugging (mechanism 4). In addition, kinetic data and data models will be reviewed.

The benefits of and potential new applications for the products of these efforts are listed in the final column of Table 2. In addition to the six listed, each plugging mechanism may result in unique pressure and flow "signatures." If the appropriate models are available, these signatures can be interpreted to help identify the plugging mechanism or to play a role in the real-time control of the process.

**Table 2. Present status and prospects for tools to analyze tank waste pipeline plugging**

| Plugging mechanism | Current predictive tools | Predictive tools, data, and data models needed | Benefits of models with enhanced capabilities and new applications |
|---|---|---|---|
| 1. Solids settling, static PSD | – Critical velocity empirical correlation, Oroskar and Turian (1980)<br>– Pressure loss, empirical correlation Wasp (1979)<br>– ESP to calculate initial composition and solid content for salt solutions | – PSD and particle shape—effects on properties and flow<br>– Viscosity and hindered settling models = f(solids volume fraction, PSD, particle shape)<br>– Integrate heat transfer analysis | – More accurate critical velocity and pressure drop<br>– Potentially higher solids content, less diluent, less carrier liquid |
| 2 Solids settling and deposition, dynamic PSD (precipitation, agglomeration, breakup) | | – Agglomeration and breakup data and models<br>– Precipitation kinetics data and models<br>– Slurry/salt flow model: 1-D or 2-D, PSD = f(composition, precipitation, agglomeration, breakup, flow, T)<br>Bed depth = f(x, t)<br>Surface interaction kinetics<br>– Viscosity and hindered settling models = f(composition, solids volume fraction, PSD, particle shape, T) | – Risk reduction by more accurate operating boundaries<br>– Avoid unstable mixtures due to flow-chemistry coupling<br>– Provide local pressure, temperature, concentrations, and bed depth<br>– Less safety margin required<br>– Less carrier liquid<br>– Provides tool to evaluate unplugging methods<br>– Minimize dilution water for salt transfers<br>– Reduce downtime required to unplug salt-well pipelines, increase availability<br>– Optimize operations<br>– Analysis of the dynamics of process upsets such as loss of pumping |
| 3 Surface deposition | | – 1-D or 2-D slurry/salt model with deposition layer = f(x,t)<br>– Surface interaction kinetics | – Predict time to plug and plug location<br>– Provides tool to evaluate prevention and unplugging methods |
| 4 Bulk or slug plugging | | – 1-D slurry/salt flow model reaction + precipitation + agglomeration = f(x,t) | – Permits identification of unstable operating conditions |
| 5 Packed bed in vertical flow | | – Terminal velocity correlation for a concentrated slurry = f(PSD, shape) | – Add to standard evaluation to avoid this type of plugging |
| 6 Deposition at elbows, constrictions, etc. | | – Tests to identify key parameters CFD with reaction + deposition + precipitation + agglomeration | – Evaluate plugging potential for transfers<br>– Evaluate connector designs |

ESP = Environmental Simulation Program.
PSD = particle size distribution.
1-D, 2-D = 1-dimensional, 2-dimensiaonal.
CFD = computational fluid dynamics.

In addition, understanding the plug formation mechanism will help in the formulation and evaluation of unplugging methods, process control design and operation, and process optimization.

TFA is conducting experimental studies at FIU to obtain data for simulated waste with a PSD representative of that of the Hanford wastes. In addition "numerical experiments" using a CFD code were conducted in 2000 and 2001 at MSU to compute critical velocities, allowing a comparison of these computed velocities with those predicted by Oroskar and Turian (1980). In addition, RPP-sponsored studies are ongoing at Hanford to evaluate the uncertainty in data on tank waste particle sizes.

Work is ongoing to measure some of these data, either by characterization of actual wastes or by measurements of simulated tank waste. TFA efforts to measure particle density, PSD, particle shape, and viscosity are ongoing at AEA Technology, FIU, MSU, and ORNL.

## 2.5 Conclusions and Recommendations

This article identifies some of the fluid dynamics and chemical modeling capabilities needed to reduce the risk of pipeline plugging during tank waste transfers at Hanford, evaluates some of the modeling tools currently in use for waste transfer analysis relative to these needs, and recommends actions to address capability gaps.

Extension and validation of the current models used to evaluate waste transfers, such as the empirical correlation of Oroskar and Turian and the ESP equilibrium chemistry code, are necessary to improve the accuracy for slurry-water transfers and to provide the initial conditions for waste transfers. The RPP and TFA are working to validate and improve these tools for analysis of the static PSD case.

Six distinct and credible waste pipeline plugging mechanisms have been identified. However, the tools currently being used by the site for design and waste transfer evaluations can directly address only one of these—development of a blockage due to solids settling from a slurry with a static PSD. The static PSD plugging mechanism is relevant for many sludge-water transfers, but models capable of assessing the other five plugging mechanisms are needed.

Current evaluations focus on (1) calculation of the critical velocity and pressure drop using empirical correlations and (2) estimation of the initial waste composition and solids volume fraction using an equilibrium chemistry model. Precipitation, gelation, other chemical reactions, particle agglomeration, particle breakup, and other dynamic processes occur in some waste transfers. Waste-surface interactions can also be important. In addition, waste chemistry and flow are coupled—chemistry affects the flow, and flow affects the chemistry. A model capable of describing these dynamic and coupled processes is needed to predict the waste behavior in four of the six plugging mechanisms.

Predictive tools developed for waste transfer analysis must ultimately be practical for implementation in the field. Application of a three-dimensional CFD model has been explored by MSU as an approach to model some dynamic effects. TFA will de-emphasize the CFD-based development path until it becomes easier to implement, faster computers become available to the design and analysis staff, and theoretical difficulties associated with bed mechanics are overcome. CFD will eventually play an increasing role in waste transport analysis, and it can now be productively applied to some specialized analyses.

Current waste transfer criteria were developed without considering all plugging mechanisms, chemical dynamics, or flow-chemistry coupling. Performing tests without the models needed to understand and apply the results will be insufficient to reduce the risk of pipeline plugging. The tank wastes are a complicated chemical system. The important complexities must be understood in order to identify the phenomena involved and to provide a description of these in practical and accurate tools.

Transport model development work in FY 2002 will focus on (1) support of salt solution transport projects and operations (e.g., the S-112 project and salt-well pumping) and (2) improvements to the hindered settling correlation to account for settling of polydispersed solids and particle shape. In early FY 2002, a literature review of alternative potential models will be published. Model requirements and a model development plan will then be developed and reported in collaboration with Hanford operations and project users. To make the models useful as early as possible in the process, the capabilities of the models will be developed and introduced incrementally. One will be a laminar flow model with dynamic PSD (mechanism #2) to describe salt solution behavior in pipelines. This model will be applied to analysis of transfers from trickle-bed saltcake dissolution and salt-well pumping operations. A second model will be a turbulent-flow model with dynamic PSD to describe sludge-slurry transfers and salt-solution transfers susceptible to bulk plugging. New kinetic data will be required for these models. The specific processes and components to be included will be selected based on an analysis of the models and the pipeline conditions to be addressed. A "bulk-thickening" model will be needed for very rapid transitions to metastable gel states. Surface interaction and metastable processes will be added to the model later (see mechanisms #3 and #4). In general, the simplest possible treatment of the velocity profile will be used. The ability to describe transient behavior will be included, at least to the extent that changes in the PSD are described. When the dynamics are relatively slow, the problem can be analyzed by making quasi-steady-state assumptions.

Collecting the right data is essential for application of the predictive models and for minimizing the cost of research, development, and waste characterization. The models should be used to help specify what types of data are required. It is likely that additional kinetic data will be needed.

## 2.6 References

Estey, S. D., and T. A. Hu 1998. *Flow Velocity Analysis for Avoidance of Solids Deposition During Transport of Hanford Tank Waste Slurries*, HNF-2728, Lockheed Martin Hanford Corporation, Richland, Washington (October).

Francis, A., J. Henshaw, M. Manning, N. Pilkington, and C. Kemp 2000. *Progress Report on Precipitation Studies of Tank Simulant Mixtures (AN-103, SRS)*, AEAT/R/NT/0285, AEA Technology, Oxfordshire, U.K. (November).

Gillies, R. G., and C. A. Shook 1991. "A Deposition Velocity Correlation for Water Slurries," *Canadian Journal of Chemical Engineering* 69, 1225–27.

Henshaw, J. 1999. *Summary of Precipitation Studies of Phosphate, Fluoride and Sulphate Solutions in Tank Wastes*, AEAT-6256, AEA Technology, Oxfordshire, U.K. (November).

Hu, M. Z., D. W. DePaoli, and D. T. Bostick 2001. *Dynamic Particle Growth Testing: Phase I Studies*, ORNL/TM-2001/100, Oak Ridge National Laboratory, Oak Ridge, Tenn (June).

Hunt, R. D., T. A. Dillow, J. R. Parrott, Jr., J. C. Schryver, C. F. Weber, and T. D. Welch 2000. *Waste Preparation and Transport Chemistry: Results of the FY 2000 Studies*, ORNL/TM-2000/298, Oak Ridge National Laboratory, Oak Ridge, Tenn.

Jewett, J. R., and L. Jensen 2000. *Assessment of Available Particle Size Data to Support an Analysis of the Waste Feed Delivery System Transfer System*, RPP-6247, CH2MHill Hanford Group, Inc., Richland, Washington (August).

Julyk, L. J., J. C. Oten, and W. L. Willis 2000. *Waste Feed Delivery Transfer System Analysis*, RPP-5346, CH2MHILL Hanford Group, Inc., Richland, Washington (May).

Kuipers, J. A. M., and W. P. M. van Swaaij 1998. "Computational Fluid Dynamics Applied to Chemical Reaction Engineering," pp. 227–319 in *Advances in Chemical Engineering*, Vol. 24.

Levenspiel, O. 1962. *Chemical Reaction Engineering*, John Wiley & Sons, New York.

Liddell, K. C., and D. F. Burnett 2000. *Critical Transport Velocity: A Review of Correlations and Models*, RPP-7185 Rev. 0, CH2MHILL Hanford Group, Richland, Washington (October).

Macosko, C. W. 1994. *Rheology: Principles, Measurements, and Applications*, VCH, New York.

Maude, A. D., and R. L. Whitmore 1958. "Hindered Settling," *British Journal of Applied Physics* 9, 477–482.

Oroskar, A. R., and R. M. Turian 1980. "The Critical Velocity in Pipeline Flow of Slurries," *AIChE Journal* 26(4), 550–58.

Richardson, J. F., and W. N. Zaki 1954. "The Sedimentation of a Suspension of Uniform Spheres Under Conditions of Viscous Flow," *Chemical Engineering Science* 3, 65–73.

Shor, J. T., and J. S. Watson 1990. "The Sedimentation of Bimodal Distributions of Unflocculated Microspheres," *Separation Science and Technology* 25, 2157–70.

Wasp, E. J., J. P. Kenny, and R. L. Gandhi 1979. *Solid-Liquid Flow Slurry Pipeline Transportation*, Gulf Publishing Company, Houston.

# 3. SLURRY SIMULANTS FOR HANFORD TANKS AY-102 AND AZ-101

Rodney D. Hunt

*Nuclear Science and Technology Division*
*Oak Ridge National Laboratory*

Since most of the cross-site transfer lines at the U.S. Department of Energy's Hanford site are no longer functional, the River Protection Project (RPP) must ensure that future slurry transfers can be safely made without any pipeline plugging. For FY 2001, the RPP has requested that researchers at Florida International University (FIU) demonstrate the viability of two proposed slurry transfers in FIU's large laboratory-scale pipeline system. RPP personnel selected their proposed slurry transfers from tanks AY-102 and AZ-101. (The total volumes of waste in tanks AY-102 and AZ-101 are 592 and 909 kgal, respectively. Tanks AY-102 and AZ-101 contain 216 and 46 kgal of sludges, respectively.) The masses of key chemical components in Tanks AY-102 and AZ-101 were obtained from the best basis inventory in the Tank Waste Information Network System (TWINS), and they are given in Table 1. For tanks AY-102 and AZ-101, the last sludge and supernatant samples were during FY 2000. It should be noted that sludge from tank C-106 was transferred to tank AY-102 prior to the last sampling.

**Table 1. Masses of key chemical components in tanks AY-102 and AZ-101**

| Chemical | Tank AY-102 (kg) | Tank AZ-101 (kg) | Chemical | Tank AY-102 (kg) | Tank AZ-101 (kg) |
|---|---|---|---|---|---|
| Aluminum | 52,000 | 45,000 | Nickel | 3,000 | 1,400 |
| Bismuth | 60 | 50 | Nitrate | 870 | 230,000 |
| Calcium | 3,900 | 670 | Nitrite | 14,000 | 230,000 |
| Carbonate | 160,000 | 110,000 | Phosphate | 16,000 | 4,100 |
| Chloride | 350 | 490 | Potassium | 1,400 | 15,000 |
| Chromium | 2,000 | 2,400 | Silicon | 1,400 | 660 |
| Fluoride | 190 | 6,700 | Sodium | 140,000 | 360,000 |
| Hydroxide | 250,000 | 170,000 | Strontium | 230 | 100 |
| Iron | 89,000 | 23,000 | Sulfate | 5,100 | 50,000 |
| Lanthanum | 940 | 950 | Total organics | 6,300 | 2,000 |
| Lead | 4,400 | 200 | Uranium | 3,300 | 1,600 |
| Manganese | 19,000 | 300 | Zirconium | 90 | 7,600 |
| Mercury | 140 | 0 | | | |

## 3.1 Simulant Formulation

The test conditions, such as flow rates, temperatures, and potential water additions, were provided by RPP personnel; the simulant (simulated waste) recipes for the proposed transfers were developed by Oak Ridge National Laboratory (ORNL) staff members. The initial step in formulating the simulant was to acquire the waste volumes and compositions from TWINS for each tank. Next, the total charge for the chemical components in Table 1 was determined. If the best basis inventory was completely accurate, then the charge balance should be zero. At ORNL, the hydroxide level was adjusted to achieve a charge balance of zero. Researchers at RPP have also demonstrated that the sodium concentration can be successfully adjusted to produce a zero charge balance, while staff members at Mississippi State University used a combination of these approaches to obtain charge balance. It should be noted that modifications to the TWINS databases are under way to address the lack of charge balance in the best basis inventories. Subsequently, water was added to chemical components in Table 1 so their combined weight would be equal to the estimate of the tank waste mass. Then the weight percentage for each of the

chemical components was determined. All components with a wt% of 0.2 or greater were included in the simulant formulation. Minor components such as fluoride were also added when they could be chemically significant. The hydroxide inventory was then increased slightly in order to compensate for anions that were no longer included. This revised tank inventory formed the basis for the compositions of the chemical simulants.

A variety of commercially available chemical compounds were selected and used in the simulant formulations. For example, aluminum nitrate and sodium metaaluminate were used as sources of aluminum, and manganese compounds include manganese dioxide and manganese sulfate monohydrate. The ratios of chemical compounds were adjusted to closely approximate the ratios in the final revision of the tank inventories. Two chemical substitutions were made in the final tank inventories because of safety and cost considerations. The behavior of sodium and nitrate should be comparable to the behavior of potassium and nitrite, respectively, and their contributions to the slurry properties should be primarily related to ionic strength. Therefore, nitrite was considered part of the nitrate and potassium was part of the sodium. It should be noted that poisonous nitrogen dioxide could form if sodium nitrite were added to undissolved aluminum nitrate in a highly caustic solution.

The initial simulant formulations are presented in Tables 2 and 3. Both of the simulants comprised three solutions. One of the solutions was acidic, and another solution was highly caustic. The third solution in each simulant recipe was slightly basic. The objective of the multiple solutions was to ensure that a portion of each chemical element or compound would be soluble during simulant formulation. The slightly basic solution and the acid sample were combined before the highly caustic solution was added to form the final formulation. It should be noted that both simulants generated nonhazardous gases such as carbon dioxide during the preparation. After the three solutions were combined, the temperature of the slurry simulant was maintained at 80°C for 1 week and 50°C for an additional week.

**Table 2. Initial and final simulant formulation for Hanford tank AY-102**

| Acidic | Slightly basic | Basic |
|---|---|---|
| 10.00g $H_2O$ | 10.00g $H_2O$ | 10.00g $H_2O$ |
| 0.50g $H_2C_2O_4 * 2H_2O$ | 0.63g $Fe(NO_3)_3 * 9H_2O$ | 0.93g $NaAlO_2$ |
| 1.75g $Fe_2O_3$ | 0.12g $MnSO_4 * H_2O$ | 1.32g $Al(OH)_3$ |
| 0.39g $MnO_2$ | 0.15g $Na_2SiO_3 * 5H_2O$ | 0.98g $Na_3PO_4 * 12H_2O * 0.25NaOH$ |
| 0.15g $CaCO_3$ | 3.77g $Na_2CO_3$ | |

**Table 3. Initial simulant formulation for Hanford tank AZ-101**

| Acidic | Slightly basic | Basic |
|---|---|---|
| 5.00g $H_2O$ | 8.00g $H_2O$ | 3.88g $H_2O$ |
| 1.92g $Al(NO_3)_3 * 9H_2O$ | 1.06g $Na_2CO_3$ | 1.13g $NaOH$ |
| 0.06g $ZrO_2$ | 0.08g $NaF$ | 0.43g $NaAlO_2$ |
| | 0.06g $Na_2SiO_3 * 5H_2O$ | |
| | 0.50g $Na_2SO_4$ | |
| | 0.11g $Na_3PO_4 * 12H_2O * 0.25NaOH$ | |
| | 0.96g $Fe(NO_3)_3 * 9H_2O$ | |
| | 2.23g $NaNO_3$ | |

After the slurry simulants were permitted to equilibrate for 2 weeks, volume percentages of gravity-settled solids for tanks AY-102 and AZ-101 were 39 and 25%, respectively. For comparison, TWINS indicates that the solid volume percentages for tanks AY-102 and AZ-101 should be 36 and 5%. Apparently, a 2-week equilibration for the tank AY-102 simulant was sufficient, but the tank AZ-101 simulant needs a longer equilibration time. It should be noted that the solid volume percentage for the

tank AZ-101 simulant continued to decrease with time. Because of the uncertainties of the solid volume percentage, the researchers at Mississippi State University used the Environmental Simulation Program (ESP) to simulate the original formulation for tank AZ-101 at 47°C. The ESP results indicated that the volume and weight percentages of the solids would be 2% and 5%, respectively, at equilibrium.

## 3.2 Viscosity Testing

After the simulants were prepared and equilibrated, a series of viscosity tests were performed on the samples. These solids in the simulants were resuspended into the solution before 16 mL of the sample was transferred into a preheated small sample adapter for the Brookfield DV-III rheometer. The sample was then permitted to equilibrate for 15 min. For each sample, two viscosity tests were performed in an effort to determine the effects of shear rate and time. During the shear rate tests, the shear rate was varied from 12 $s^{-1}$ to 49–122 $s^{-1}$ to 12 $s^{-1}$. A particular shear rate was maintained for a period of 2 min before it was increased or decreased by an increment of 12 $s^{-1}$. The viscosity of the tank AY-102 sample decreased significantly as the shear rate was increased. For example, the viscosities of the tank AY-102 simulant at 50°C were 17 and 9 cP at shear rates of 24 and 73 $s^{-1}$, respectively. In sharp contrast, the viscosities of the tank AZ-101 simulant at 50°C were 2.9 and 2.4 cP at shear rates of 24 and 73 $s^{-1}$, respectively. In the time tests, a shear rate of 49 or 61 $s^{-1}$ was applied to the sample for 5 min. The simulants were then cooled to 45 and 40°C, and the viscosity tests were repeated at both temperatures. For the tank AY-102 simulant, the viscosities at 50, 45, and 40°C were 10, 11, and 11 cP, respectively, at a shear rate of 49 $s^{-1}$. For the tank AZ-101 sample, the viscosities at 50, 45, and 40°C were 2.6, 3.4, and 3.7 cP, respectively, at a shear rate of 61 $s^{-1}$.

These viscosity results were presented to RPP and Tank Focus Area staff members, and they agreed that no further modifications to the tank AY-102 simulant were needed before the larger-scale tests at FIU. However, the initial formulation of the tank AZ-101 slurry did not appear to present a sufficient challenge for the waste transfer tests at FIU. Therefore, the amount of water in the sample was systematically reduced, and the viscosity of the modified simulant was determined as a function of temperature. These viscosity results are presented in Table 4.

**Table 4. Viscosity of the tank AZ-101 simulant as a function of temperature and water loss**

| Water loss from original formulation (g) | 50° | 45° | 40° |
|---|---|---|---|
| 0 | 2.6 cP | 3.4 cP | 3.7 cP |
| 2 | 3.3 cP | 3.6 cP | 3.9 cP |
| 4 | 3.6 cP | 4.8 cP | 4.9 cP |
| 6 | 5.4 cP | 6.4 cP | 7.0 cP |

After further discussions with RPP personnel, it was decided that 6 g of water should be removed from the original formulation prior to the tests at FIU. The revised formulation for the tank AZ-101 simulant is presented in Table 5. A new sample based on the final formulation of the tank AZ-101 simulant was prepared, and the viscosity results were as expected. The particle size distributions for both final simulants were measured at FIU. The mean particle sizes for tanks AY-102 and AZ-101 simulants were 120 microns and 150 microns, respectively. Previously, RPP studies on actual slurries indicated that these mean particle sizes are quite reasonable. Finally, an ESP simulation on the final simulant for tank AZ-101 indicated that the solid phase would consist of gibbsite, iron (III) hydroxide, sodium fluoride-sodium sulfate double salt, and zirconium oxide. In addition, the ESP predictions for viscosity, percentage solids by volume, and percentage solids by weight at 20°C were 5 cP, 4%, and 7%, respectively.

**Table 5. Final simulant formulation for Hanford tank AZ-101**

| Acidic | Slightly basic | Basic |
|---|---|---|
| 3.00g $H_2O$ | 6.00g $H_2O$ | 1.88g $H_2O$ |
| 1.92g $Al(NO_3)_3 * 9H_2O$ | 1.06g $Na_2CO_3$ | 1.13g NaOH |
| 0.06g $ZrO_2$ | 0.08g NaF | 0.43g $NaAlO_2$ |
| | 0.06g $Na_2SiO_3 * 5H_2O$ | |
| | 0.50g $Na_2SO_4$ | |
| | 0.11g $Na_3PO_4 * 12H_2O * 0.25NaOH$ | |
| | 0.96g $Fe(NO_3)_3 * 9H_2O$ | |
| | 2.23g $NaNO_3$ | |

# 4. PARTICLE AGGLOMERATION BEHAVIOUR THEORY AND EXPERIMENT APPLICABLE TO THE HANFORD WASTE STORAGE FACILITY[*]

Elizabeth Allan, Tony Francis, Jim Henshaw, Paul Smith, and Steven Swanton

*AEA Technology*
*B220 Harwell, Didcot*
*Oxfordshire*
*OX11 0RA*
*UK*
*Telephone 44 (0)1235 435843*
*Facsimile 44 (0)1235 436314*

## Abstract

This report outlines the work taking place this year as part of the Tanks Focus Area chemistry program being carried out by AEA Technology in the United Kingdom. The focus of the first year of this 2-year program has been to understand particle agglomeration processes relevant to the Hanford waste tanks. Agglomeration is important because it controls the size of sludge particles during pipe transfers and processing, a key factor in pipe blockages and process times during liquid-solid separations. The theory of agglomeration, de-agglomeration, and particle settling and resuspension has been reviewed and is discussed here. At the high ionic strengths in the waste tanks, agglomeration is inevitable. The important factors contributing to the rate of agglomeration and final size of the agglomerate are the primary particle properties and the turbulent energy density dissipation rate. The system comprising gibbsite, boehmite, $Fe(OH)_3$, and $SiO_2$ is a simple representation of the sludge contained in the Hanford tanks C-103 and C-104, which are the focus of the experimental study. The experiments that are currently in progress on these mixtures are also described, and some preliminary results from the light scattering experiments are presented. These indicate that no agglomerates larger than 120 μm are observed and that the mean agglomerate size falls with increasing shear rate.

## 4.1 Introduction

Many of the waste storage tanks at the U.S. Department of Energy's Hanford site contain large amounts of aggregated colloidal material (sludge) which will need processing. Steps involved in tank waste remediation processes include sluicing to create waste suspensions, transporting the suspensions via pumping to central processing facilities, washing and leaching, and separating particles from supernatant liquids to form high- and low-level waste streams. Rapid sedimentation velocities are desired to allow solid liquid separations within reasonable time frames and, for these large particles, are desirable. Conversely, to prevent the formation of blockages in the transfer lines, settling is an undesirable phenomenon and therefore small particles are desirable. The velocity of the waste required to suspend and transport the solid fraction of the waste (the "critical velocity") has been determined for each anticipated transfer, and the pipeline pressure required to achieve the critical velocity has also been determined. Uncertainties in the particle size distribution have resulted in estimates for required pipeline pressures that greatly exceeded the design limits (Jewett et al. 2000).

---

[*] This section is a condensed summary of AEA Technology's FY 2001 work. Please see AEAT/R/NS/0516, *Particle Sizing Studies on Tanks C-103 and C-104 Simulants Under Varying Flow Conditions*, (in preparation), and Henshaw and Smith (2001) for details.

It is therefore important to understand agglomeration processes and the effect on particle size for chemical systems and conditions of relevance to the Hanford site. In this respect, one of the key unresolved issues is the extent to which agglomerates would be present during transfer and the extent to which agglomerates will be diminished by turbulence. It is also not clear what the time scale is for the re-formation of the agglomerates after turbulent break-up. In order to address these issues, a two-year program of work has been started, the first year of which is coming to completion. This paper outlines some of the work that has been carried out in this first year.

## 4.2 The Theory of Particle Agglomeration

A review of particle agglomeration has been written to identify the main mechanisms for particle agglomeration and de-agglomeration (Henshaw and Smith 2001). This review focused on the open literature data on colloidal particle agglomeration and included electronic searches of Chemical Abstracts and the International Nuclear Information System (INIS) Databases (IAEA 1998). The review did not cover issues such as crystallization, which involve nucleation and primary particle growth, since it is assumed that for the tank sludge precipitation is complete and what is of interest is the behavior of the existing aggregated material. The review points out that at the high pH and ionic strengths likely to exist in the tanks, colloidal material will aggregate. From the review, the main equation describing the behavior of particles passing along a pipe is identified as

$$\frac{dn_k}{dt} = \frac{1}{2}\sum_{\substack{i=1 \\ j=k-i}}^{k-1} a_{i,j}n_i n_j - n_k \sum_{i=1}^{N-k} a_{i,k}n_i + \sum_{i=1}^{N-k}(1+\delta_{i,k})b_{i,k}n_{k+i} - \frac{1}{2}\sum_{i=1}^{k-1}(1+\delta_{i,k-i})b_{i,k-i}n_k - c_k n_k + d_k \quad , \quad (1)$$

where $n_k$ is the particle number density of a particle consisting of $k$ primary particles, $N$ is the largest particle size allowed in the system, $a_{i,j}$ are the agglomeration rate constants, $b_{i,j}$ are the de-agglomeration rate constants, $c_k$ is the rate at which particles deposit on the pipe wall, and $d_k$ is the rate at which particles are re-suspended. The first term in this equation corresponds to agglomeration of particles smaller than size $k$ to form a particle containing $k$ primary particles. The second term is the loss of particles of size $k$ due to agglomeration to form larger particles. The third term represents formation of particles from larger particles by de-agglomeration and the fourth term is loss of the particle due to its break-up. The last two terms represent deposition and re-suspension of the particles to and from the pipe wall. Particle agglomeration, de-agglomeration, and deposition therefore can be appreciated and understood if the constants $a$ to $d$ in Eq. (1) are known for the particular situation of interest. The review identified three terms contributing to the agglomeration rate constants:

$$a = a_{Brownian} + a_{Turbulent} + a_{Gravitional} \tag{2}$$

The first is due to simple Brownian motion, that is the continuous random movement (or diffusion) of particles suspended in a fluid. Brownian agglomeration occurs when, as a result of their random motion, particles collide and stick together. Brownian agglomeration is probably the best understood of the agglomeration mechanisms. The turbulent agglomeration term is usually split into two contributions, shear and inertial terms. Turbulent shear causes particles following flow path lines to collide with one another. This occurs because particles on different streamlines are travelling at different speeds. Turbulent shear agglomeration is a result of this effect. Turbulent inertial agglomeration results when particle trajectories depart from flow streamlines and such departures cause collisions. The final term in Eq. (2) is due to gravitational agglomeration. Gravitational agglomeration occurs as a result of the size dependence of the terminal velocity of small particles. The slowly settling (generally smaller) particles are captured by the more rapidly settling (generally larger) particles.

Expressions are given in Henshaw and Smith (2001) for the various terms in Eq. (2) and these are summarized here. The Brownian term can be written as

$$a_{i,j}^{Brownian} = \frac{2k_B T}{3\mu}(r_i + r_j)\left(\frac{1}{r_i} + \frac{1}{r_j}\right)F \tag{3}$$

where $k_B$ is the Boltzmann constant, $T$ the temperature, $\mu$ the viscosity of the liquid and $r$ the radius of the colliding particles. The term $F$ accounts for a number of elements which could be a slip factor (accounting for fluid slip around the particle), a shape factor (particle nonspherical) and a collision efficiency/stability factor (accounting for the primary particle interaction forces, see for example Rector and Bunker (1995). Each of these factors is discussed in Henshaw and Smith (2001), but in general terms they are determined by matching an agglomeration model with experimental data.

For turbulent shear Bixler (1998) gives the following expression for the agglomeration term:

$$a_{i,j}^{Turbulent} = \theta_s \vartheta_{PK}(r_i, r_j)\chi_c{}^3[r_i + r_j]^3\sqrt{\frac{8\rho_f \pi \varepsilon}{15\mu}} \tag{4}$$

where
$\theta_s$ is the dimensionless particle to particle sticking efficiency,
$\theta_{PK}$ is the dimensionless collision efficiency correction factor,
$\chi_C$ is the dimensionless collision shape factor,
$\rho_f$ is the fluid density,
$\varepsilon$ is the turbulent energy density dissipation rate.

For gravitational agglomeration the following expression has been used by Fuchs (1964):

$$a_{i,j}^{Gravity} = \pi y_c^2(r_i, r_j)|v_s(r_i) - v_s(r_j)| = \pi(r_i + r_j)^2 \varepsilon_G(r_i, r_j)|v_s(r_i) - v_s(r_j)| \tag{5}$$

where $y_c$ is the initial separation of particles which leads to grazing contact and $v_s$ is the settling velocity of a particle of radius $r$. The following analytic expression for the gravitational collision efficiency was used:

$$\varepsilon_G = \frac{3(r_i/r_j)^2}{2(1 + (r_i/r_j))^2} \tag{6}$$

where $r_j \geq r_i$.

This model has been applied to aerosol behaviour and so has only been tested for particles in a gaseous fluid. When viscous drag forces are large, as in a liquid, $a^{Gravity}$ may not be important.

Henshaw and Smith (2001) discuss in more detail the various models for agglomeration, with the conclusion that Brownian agglomeration is well understood but both turbulent and gravitational agglomeration are not.

In order to describe de-agglomeration, the theory of Mean (1978)is outlined in Henshaw and Smith (2001). This theory leads to various expressions for the rate constant $b$ in Eq. (1), depending on the particle size and flow conditions. Means defines the break-up rate $b_k$ by

$$\frac{dn_k}{dt} = -b_k n_k \ .$$

(7)

For agglomerates in the bulk of the fluid, the break-up rate is controlled by the eddy frequency, which leads to the following expressions for the de-agglomeration rate constant:

$$b_k = \sqrt{\frac{\varepsilon}{\upsilon}} : \qquad 2r_k < \lambda_0$$

(8)

$$b_k = \left(\frac{\varepsilon}{4r_k^2}\right)^{1/3} : \quad 2r_k > \lambda_0$$

(9)

where the Kolmogorov microscale of turbulence for the smallest eddies is given by

$$\lambda_0 = \left(\frac{\upsilon^3}{\varepsilon}\right)^{1/4} \ ,$$

(10)

and $\upsilon$ is the kinematic viscosity of the fluid.

For agglomerates entering the boundary layer, the de-agglomeration rate is given by

$$b_k = k\frac{A}{V}$$

(11)

where $k$ is the mass transfer rate constant to the pipe surface of area $A$ and volume $V$.

The theory outlined by Means (1978) leads to expressions for the maximum possible particle diameter, the critical value of the energy density dissipation rate above which agglomerates are unstable, and, in the boundary layer, the critical friction velocity above which agglomerates are unstable. These expressions are reproduced in Henshaw and Smith (2001), but as an example, the expressions for the maximum agglomerate size are given here:

$$d_{max} = \left(\frac{12\mu\pi a^2}{F_A}\right)^{3/2} \sqrt{\varepsilon} : \qquad \lambda_0 < d_{max} < 10\lambda_0$$

(12)

$$d_{max} = \left(\frac{2F_A}{\pi a^2 \rho_f}\right)^{3/2} \frac{1}{\varepsilon} : \qquad d_{max} > 10\lambda_0$$

(13)

where *d* is the particle diameter, *a* is the primary particle size, and $F_A$ is the mean attractive force holding two primary particles together. Hence, these terms, along with the energy density dissipation rate, control the agglomerate size. In simple terms, agglomerate size is a balance between the Van der Waals forces holding the particles together and the fluid turbulent shear forces. The Van der Waals force between particles is characterized by the Hamaker constant, and for a number of colloidal materials, these have been measured (Fennell and Wennerström 1999). The theory of particle break-up proposed by Means (1978) is simple and applicable. However it has two problems: (1) it needs to be generalized to non-spherical agglomerates, and (2) it requires experimental validation.

The final two terms in Eq. (1) are not discussed in Henshaw and Smith (2001) but will be discussed here briefly. The deposition and re-suspension of particles on pipes in flowing systems has been studied by a number of groups [Beal (1970, 1978); Bowen and Epstein (1979); and Zimmer and Dahneke (1976)]. Beal derived extensive empirical correlations for the deposition rate of particles (different size ranges, different materials, gas and liquid fluids, etc.) based on his own and others' experimental studies. From the work of Beal, the deposition rate constant is given by

$$c = \frac{K.p.v_r}{K + p.v_r} \tag{14}$$

where *K* is the transport coefficient, $v_r$ is the radial velocity of the particle, and *p* is the sticking probability. The terms *K, v* and *p* are complicated functions of a dimensionless stopping distance $S^+$, a Fanning friction coefficient $c_f$, and the particle diffusion constant *D.* For example

$$K = U\sqrt{\frac{c_f}{2}}\left\{4.83(\frac{v}{D})^{2/3}F(\frac{v}{D},S^+) - 140.17(\frac{v}{D})^{1/3}G(\frac{v}{D},S^+) + H(v,D,c_f)\right\} \tag{15}$$

where *U* is the linear flow velocity along the pipe and the functions *F*, *G*, and *H* are complicated expressions defined by Beal (1970, 1978). The stopping distance, and therefore the deposition rate, is a function of the Reynolds number for the flow, particle diameter, and particle density. These theories allow the use of algebraic expressions to calculate both the deposition and re-suspension rates. Some knowledge of the particle-surface interaction potential is often required, but this can be parameterised if enough experimental data on deposition rates are available.

Some idea of the relative rates of agglomeration and de-agglomeration can be appreciated by applying some of the equations previously mentioned, although the details of the size distribution can only be obtained by solving Eq. (1). In comparing relative agglomeration and de-agglomeration rates, it must be noted that agglomeration is a second-order process, while de-agglomeration is first order in the particle number density. This means the de-agglomeration rate, *b*, as defined by Eqs. (8), (9), and (11), should be compared with the agglomeration rate *a.n*, where n is the particle number density. For a pipe 3 in. in diameter, with fluid flowing at 6 ft s$^{-1}$, containing 20% solids, the de-agglomeration rate is likely to be of the order of 10 s$^{-1}$ [using Eq. (8)]. The Brownian agglomeration rate [assuming *F* in Eq. (3) is 1] will be of the order of $10^2$ s$^{-1}$ for 100-nm particles and $10^{-6}$ s$^{-1}$ for 100-μm particles. These values assume the normal properties of water for the fluid. These simple calculations indicate that at the high end of the particle size distribution, de-agglomeration is orders of magnitude faster than agglomeration during a pipe transfer and will be forcing the particle size distribution to the low end of the spectrum. Detailed calculations and experiments, though, are required to quantify this behaviour properly.

### 4.3 Experimental Program on Agglomeration

*A Review of Particle Agglomeration* (Henshaw and Smith 2001) identified the important parameters to measure in order to understand agglomeration and settling. Clearly, knowledge of the primary particle size is necessary, as this and the primary particle interaction force control the maximum possible particle size. From the following discussion, we shall see that this term also influences the density of the agglomerated material. Also of importance is the "degree" of turbulence in the system as characterized by the energy density dissipation rate. The experiments that are currently under way are therefore designed to measure these properties and also provide relevant experimental data for the transport of sludges at the Hanford site.

The types of experiments that are relevant are studies of agglomerate particle size under turbulent mixing conditions. Several groups have performed such studies; see for example Kobayashi, Adachi, and Ooi (1999), Spicer and Pratsinis (1996), Oles (1992), and Serra and Casamitjana (1998). The key problem in carrying out such experiments is determining the initial volume fraction and particle size. Most of the experiments that have been carried out to look at the effect of turbulence on agglomerate size use latex particles. This is because a known quantity of 1- to 2-$\mu$m particles can be added to the liquid and hence the initial volume fraction and size distribution are known. The primary particle size is also constant. These are important parameters to know in order to determine the fractal dimension, $D$, of the agglomerates. For a solid particle, the mass of the particle scales as $r^3$; but in the case of agglomerates, the mass scales as $r^D$, where the fractal dimension $D$ is $< 3$. In order to know the settling rate, the density of the particle must be known (in the Beal model discussed earlier, $S^+$ is a function of particle density) and hence $D$ is required. If laser particle sizing is being used to measure a characteristic floc diameter, $d_m$, and relative volume fraction, $V_m$, then these are related to the initial volume fraction $V_i$ and primary particle size, $d_i$, by Serra and Casamitjana (1998):

$$V_i/V_m = (d_m/d_i)^{D-3} \ .$$  (16)

Knowing all the terms $V_i$, $V_m$, $d_m$, and $d_i$ allows the calculation of $D$, which can also be considered as a measure of the open volume of the agglomerate. Instead of using laser scattering to measure particle sizes, Kobayashi, Adachi, and Ooi (1999) examine a sample of the solution with an optical microscope and count the number of particles and their sizes. Again, they use latex particles; and, knowing the initial number $N_i$ and primary particle diameter, they estimate $D$ from

$$N_i = \sum_{n=1}^{N_f} (d_n / d_i)^D$$  (17)

where $N_f$ is the total number of flocs and $d_n$ denotes flocs of a given diameter. In the present work, laser particle sizing is being used to study the agglomerate sizes, so Eq. (16) will be used to determine $D$. The problem of determining the initial volume fraction and particle sizes is discussed below.

One approach that can be used to generate agglomerated material is to precipitate the colloidal material out of solution and then study this freshly precipitated material. From the discussion, it is clear, though, that the volume fraction and primary particle size for this precipitated material would be required, and this would be relatively difficult to obtain. The preferred alternative approach, which is being adopted in these studies, is to use materials at the start of the experiment with well-characterised particle sizes. This was the approach of LaFemina (1995) and of Rector and Bunker (1995) in their studies on the simulant C-103.

The materials that are being used in this study are SpaceRite-S11 gibbsite powder supplied by Alcoe Corporation, nominal particle size 0.25 $\mu$m; Dispersal P2 boehmite powder, supplied by Condea Ltd.,

nominal particle size 10 nm; $Fe(OH)_3$ slurry (13 wt%) supplied by NOAH Tech Corporation, nominal particle size 0.5 μm; and Syton-W30 $SiO_2$ slurry (wt 30 wt%), supplied by Morrisons Ltd., nominal particle size 80 nm. These materials are mixed in the appropriate proportions, corresponding to their ratios in tanks C-103 and C-104, with a 1 $M$ $NaNO_3$ solution at pHs in the range 10 to 14. The problem with this approach is that adding the various powders to high-pH solutions may cause them to dissolve, so that the primary particle size in solution would not be constant. However, previous work on gibbsite dissolution indicates the extent of aluminum oxide dissolution is likely to be small; also, gibbsite dissolution is inhibited by the presence of silicate, which will be present here (Henshaw et al. 1999). This is probably also true for boehmite. However, to test that this is the case, the primary particle size change is being estimated by examining the particle sizes using small amounts of solid material in solutions of $NaOH/NaNO_3$ (1 Molar) using photon correlation spectroscopy (PCS). PCS is a standard technique for measuring particle sizes of down to 2 nm in solution.

Two sets of light scattering experiments on mixtures of these oxides, corresponding to C-103 and C-104, are being performed in a stirred vessel. These experiments are starting at low volume fractions (<0.01%) and gradually increasing. The proportions of the four materials, gibbsite, boehmite, $Fe(OH)_3$ and $SiO_2$, reflect their fractions in tanks C-103 and C-104. The C-103 system has been studied before (LaFemina 1995) and represents a system higher in iron than aluminum. The C-104 system, on the other hand, reflects sludge containing more aluminum than iron. The solid material is added to a solution of $NaNO_3$ and NaOH made up to be 1 $M$ $NaNO_3$ at pHs of between 10 and 14.

The light scattering experiments are being carried out in a baffled stirred tank with a six-blade impeller as described by Spicer and Pratsinis (1996). The average shear rate, $G$, for a vessel and propeller with this geometry is given by

$$G = \left(\frac{\varepsilon}{\nu}\right)^{1/2} \tag{18}$$

where $\varepsilon$ is the energy density dissipation rate and $\nu$ is the kinematic viscosity. The energy density dissipation rate for the vessel and propeller is given by

$$\varepsilon = \frac{PN^3D^5}{V} \tag{19}$$

where $N$ is the impeller speed, $D$ its diameter, and $V$ the volume of the tank. $P$ is the impeller power number and is a function of rotational Reynolds number; it is given in Holland and Chapman (1996) as

$$P = 74.5.Re^{-1} \tag{20}$$

where the rotational Reynolds number is defined by

$$Re = \rho ND^2/\mu \ . \tag{21}$$

The equipment was calibrated with water for which the kinematic viscosity is known, and from this the kinematic viscosity of the mixtures was estimated. Measuring the propeller rate during the course of the experiments gives the energy density dissipation rate.

To carry out the analysis, a sample of the material is taken periodically from the stirred vessel, diluted, and placed in a cell for particle sizing. For dilution, a saturated solution is used to stop any problems

associated with dissolution of the material. Dilution is carried out to halt the aggregation/de-aggregation process. The time between sampling and analysis is also kept to a minimum.

A typical set of experimental results is shown in Fig. 1 for the C-103 simulant mixture at a mass fraction of approximately 12%. These are the steady state distributions obtained sampling approximately 5 minutes after mixing.
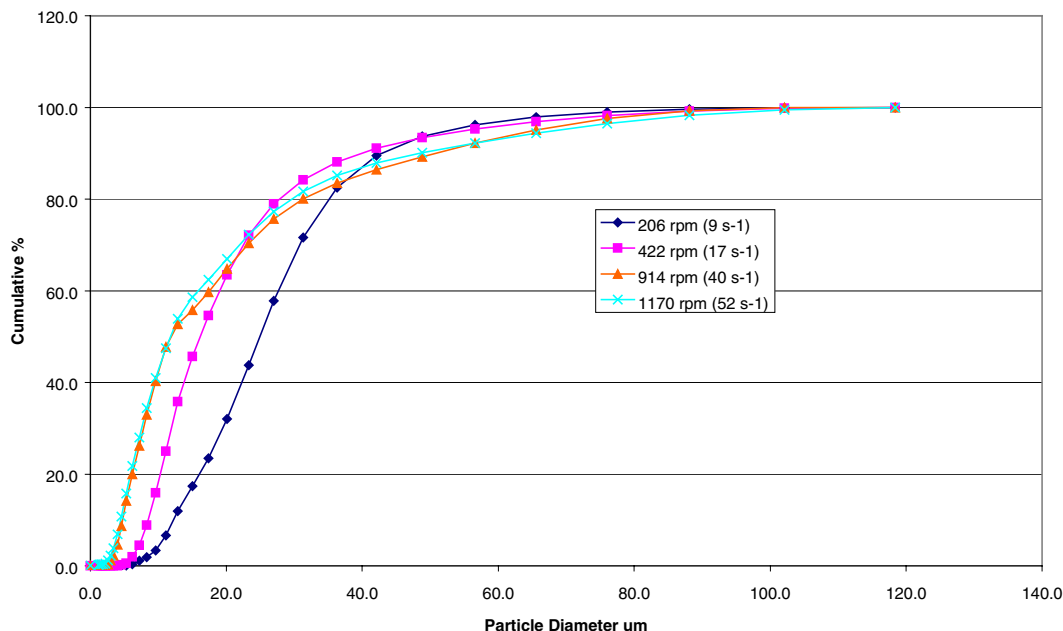


**Fig. 1. Cumulative particle size distribution for the C-103 simulant at 12% mass fraction.**

The relative mass fractions of the $SiO_2$, gibbsite, boehmite, and $Fe(OH)_3$ in this mixture are 45:1:8:386, and the pH of the solution was 12.7. Figure 1 shows a clear fall in particle size as the propeller rate increases from approximately 200 to 1200 rpm, corresponding to shear rates [using Eqs. (18) to (21)] from approximately 10 to 50 $s^{-1}$. The particle size distribution at the two lowest shear rates for this mixture is given in Fig. 2.

Figures 1 and 2 both indicate that the largest agglomerates observed in these mixtures are of the order of 120 μm; they are only a small proportion of the agglomerate particles. It is also clear that the mean particle size falls as the shear rate increases. For a 3-in. diameter pipe, with fluid flowing at 6 ft $s^{-1}$, typical plant conditions, the shear rate will be of the order of 10 $s^{-1}$ and a small fraction of particles in the 100- to 120-μm size range might be expected. This is approximately one-third the minimum eddy size, approximately 300 μm, for the flow at 200 rpm [from Eq. (10)]. Since, for a linear pipe, shear is roughly proportional to velocity to the power of 1.5, from Fig. 1 a significant drop in the average agglomerate size might be expected if the flow rate were doubled; but further increases in flow rate would have less of an effect.

### 4.4 Conclusion

The agglomeration of colloidal particles is an important issue for the processing of nuclear waste material at the Hanford site. Small agglomerates are required to facilitate pipe transfers, while large agglomerates
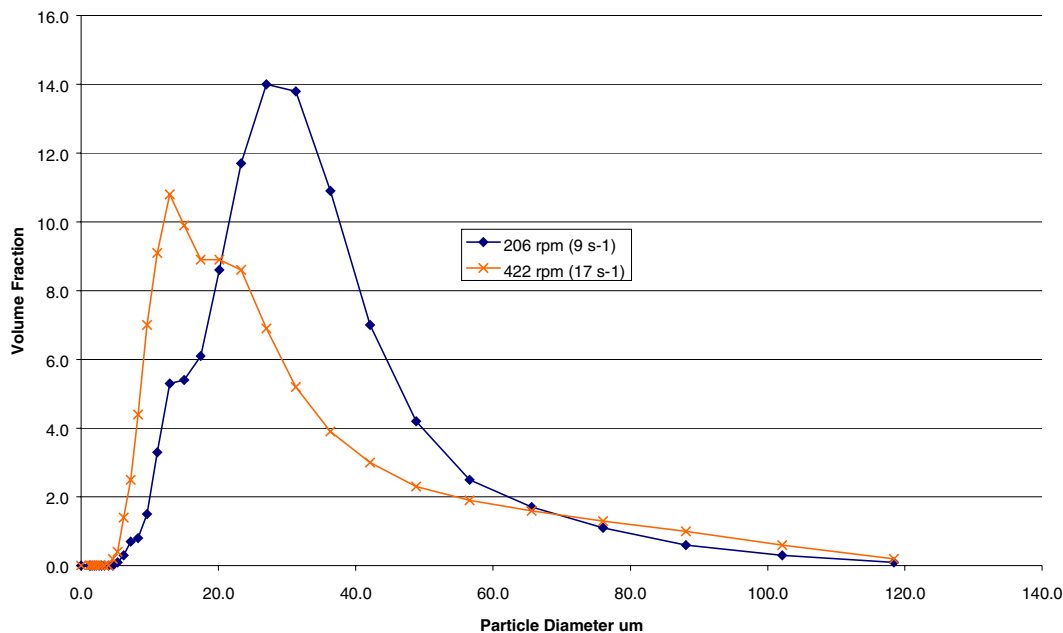
**Fig. 2. Particle size distribution for C-103 simulant mixture at two different shear rates.**

are beneficial to solid–liquid separation processes. It is therefore important to understand the mechanisms of agglomeration and de-agglomeration of materials relevant to Hanford sludge.

The theory of agglomeration mechanisms has been discussed, in which three mechanisms for agglomeration have been specified: Brownian, turbulent and gravitational. Of these three mechanisms, Brownian agglomeration is the best understood. The theory of Means (1978) has been outlined as a method of quantifying the process of de-agglomeration. The de-agglomeration rate is a function of the frequency and size of turbulent eddies. This leads to various expressions for the rate of de-agglomeration, which are function of the turbulent energy density dissipation rate, primary particle size, and interaction force. The work of Beal (1970, 1978) on particle settling and re-suspension has also been mentioned and the dimensionless stopping distance introduced. This dimensionless number is critical to the settling and re-suspension of particles and is a function of particle size and density.

The key parameters controlling particle behaviour have therefore been identified as primary particle size, primary particle interaction force, fractal dimension of the agglomerate, and turbulent energy dissipation rate of the fluid. Two sets of experiments are currently in progress to measure these terms. The first set of experiments uses PCS to measure the primary particle size and how this may change with the pH of the solutions. The second set of experiments uses particle light scattering to measure particle size and number density. The solutions for the light scattering experiments are obtained from a mixture, contained in a stirred vessel, containing a mixture of gibbsite, boehmite, $Fe(OH)_3$, and $SiO_2$. The correlation between propeller speed and turbulent energy density dissipation rate is known for the particular design of propeller and vessel being used. The mixtures that are being used in these experiments correspond to the mixtures in tanks C-103 and C-104 at Hanford. Some preliminary results from the light scattering experiments have been presented, and these indicate that no agglomerates larger than 120 µm are observed and that the mean agglomerate size falls with increasing shear rate.

## 4.5 References

Allan E., J. Henshaw, and P. Smith 2001. *A Review of Particle Agglomeration*, AEAT/R/PSEG/0398, Harwell, Oxfordshire.

Beal, S. K. 1970. "Deposition of Particles in Turbulent Flow on Channel or Pipe Walls," *Nucl. Sci. Eng.*, **40,** p. 1.

Beal, S. K. 1978. "Correlations for the Sticking Probability and Erosion of Particles," *J. Aerosol Sci.*, **9,** p. 455.

Bixler, N. E., 1998. *VICTORIA 2.0: A Mechanistic Model for Radionuclide Behaviour in a Nuclear Reactor Coolant System Under Severe Accident Conditions*, NUREG/CR-6131 (December).

Bowen, B. D., and N. Epstein 1979. "Fine Particle Deposition in Smooth Parallel Plate Channels," *J. Colloid and Interface Sci.*, **72**, p. 81.

Fennell, D., and H. Wennerström 1999. *The Colloidal Domain*, 2nd ed., Wiley-VCH, Weinheim, Germany.

Fuchs, N. A. 1964. *The Mechanics of Aerosols*, Pergamon, New York.

Henshaw, J., N. Pilkington, P. Cake, and I. Vatter 1999. *Kinetics of Sludge Dissolution: Dissolution Rates of Gibbsite Progress*, AEAT-5440, Harwell Labs, Oxfordshire, U.K.

Holland, F. A., and F. S. Chapman 1966. *Liquid Mixing and Processing in Stirred Tanks*, Reinhold.

Jewett, J. R., and L. Jensen 2000. *Assessment of Available Particle Size Data to Support an Analysis of the Waste Feed Delivery Transfer System*, RPP-6247, CH2MHill, Hanford Group, Inc., Richland, Washington (August).

Kobayashi M., Y. Adachi, and S. Ooi 1999. "Breakup of Fractal Flocs in a Turbulent Flow," *Langmuir* **15**, p. 4351.

LaFemina, J. P., 1995. "Tank Waste Treatment Science Task Quarterly Report for January–March 1995," PNL10763, Pacific Northwest National Laboratory, Richland, Washington (April).

Means, F A., 1978. *The Formation and Break-up of Corrosion Product Agglomerates in the Primary Coolant of Water Reactors*, CEGB Report RD/B/N4268, Berkley Labs, Gloustershire, U.K.

Oles, V., 1992. "Shear-Induced Aggregation and Breakup of Polystyrene Latex," *J. Colloid and Interface Sci.*, **154**(2), p. 351.

Rector, D. R. and B. C. Bunker 1995. *Effect of Colloidal Aggregation on the Sedimentation and Rheological Properties of Tank Waste*, PNL-10761, Pacific Northwest National Laboratory, Richland, Washington (September).

Serra, T., and X. Casamitjana 1998. "Structure of the Aggregates During the Process of Aggregation and Breakup Under a Shear Flow," *J. Colloid and Interface Sci.*, **206**, p. 505.

Spicer, P. T., and S. E. Pratsinis 1996. Shear-Induced Flocculation: The Evolution of Floc Structure and Shape of the Size Distribution at Steady State," *Water Research*, **30**(5), p. 1049.

Zimmer, S. L., and B. E. Dahneke 1976. "Resuspension of Particles: The Range of Validity of the Quasi-Stationary Theories," *J. Colloid and Interface Sci.*, **54**, p. 329.

# 5. SOLIDS FORMATION AND FEED STABILITY DURING WASTE SLURRY TRANSFER[*]

Rubén Darío López and Rajiv Srivastava

*Hemispheric Center for Environmental Technology*
*Florida International University*
*Miami, FL 33174*

## Abstract

Waste slurry transport operations at the Department of Energy's (DOE's) Hanford site have been disrupted by pipeline plugging on occasion. Settling of solids from the slurry or solids and gel formation during transport may have contributed to this plugging. Waste transfer conditions that could lead to pipeline plugging should always be avoided. Tests are being conducted in a pipe flow loop using simulated tank wastes to demonstrate that plug-free transfers can be accomplished for a variety of Hanford wastes under normal operating conditions. In addition, the pipe loop tests are being used to locate the limiting slurry compositions, the pipeline operating conditions and the ambient conditions for plug-free transfers. Such an "operating envelope" will aid in the staging of wastes, the design of transfer lines, and the specification of operating conditions, for waste transfers. Planned transfers can be validated in the test loop.

In FY 2001, we conducted flow experiments with Hanford tanks simulants AZ-101 and AY-102. The experiments included measurements of the solids particle size distribution (PSD) to estimate the effect of pump shearing on PSD and rheology measurements. We have also conducted experiments to study the kinetics of particle growth of a simple three-species (hydroxide-phosphate-fluoride) system in both a static (batch) and a dynamic (flow) system under different conditions (temperature and flow velocity). In addition, the pressure gradient along a horizontal pipe section and across a 90° bend was measured using a simulant with a well-characterized, static PSD to compare with the Wasp (1978) slurry transport model. A sand-and-water slurry with a PSD based on a composite of Hanford waste (median of 250 μm and Rosin Rammler coefficient of 1.7) was utilized in these latter tests. Chemical and mechanical unplugging methods to remove a plug formed due to solids formation in a sodium phosphate system were also evaluated.

Salient findings of this study include these:

- Even under the worst flow conditions, which included pump stoppage and overnight runs, both simulated AZ-101 and AY-102 wastes flowed without plugging the lines.
- The simulants showed a non-Newtonian Bingham plastic rheological behavior. This is consistent with data found in the literature. Bingham plastic viscosity models should be used in the waste transfer analysis.
- Particle size distribution (PSD) analyses showed a particle mean size of 100 to 200 μm in most samples. Particle agglomeration was observed. The particle size range is consistent with the findings of Jewett and Jensen (2000).

---

[*] This section is a condensed summary of FIU's FY 2001 work. Please see Ebadian, López, and Srivastava (2002).

- Needle-like crystals of sodium phosphate were formed. The size and the number-density of the crystals increased as the temperature decreased. The rate of crystal growth rate was fairly independent of the size of the crystals. The crystals can grow up to 1–2 mm in length in a matter of a few hours. Formation of these solids can thus be an issue in salt solution transfers at low flow rates.
- The particle growth rate was lower in a flowing system than a quiescent system. Thus flow decelerates particle growth.

## 5.1 Introduction

The tasks for FY 2001 involved the investigation of the flow behavior of surrogate wastes stored at DOE's Hanford site. The main activities included bench- and pilot-scale flow loop studies with Hanford simulated wastes (for Tanks AZ-101 and AY-102), study of rate of solid formation, pressure drop across a bend, and unplugging studies. Activities were performed according to a test plan (HCET 1999) prepared by Florida International University's Hemispheric Center for Environmental Technology (FIU-HCET). The test plan was reviewed and agreed to by the Tanks Focus Area (TFA) pretreatment waste transport stability study collaborators at Oak Ridge National Laboratory (ORNL) and by James Jewett, the liaison between the River Protection Project (RPP) and TFA.

Plugging has hampered waste slurry transport operations at DOE's Hanford and Savannah River sites. The pipelines become plugged when solids settle, adhere to the wall, or form rapidly under certain operating conditions. This project addresses the effects of temperature, flow regime, slurry composition, and chemical and physical processes on slurry transfer behavior. The main objectives of the project are as follows:

- Identifying the operating parameters and feed conditions that cause solids formation and pipeline plugging.
- Obtaining correlation of the observed data that will enable the prediction of slurry transport characteristics.
- Providing engineering data and technical recommendations to support the Hanford Tank Waste Remediation System operation.

## 5.2 Flow Loop Study with Hanford Simulants

Bench- and pilot-scale flow loop studies with simulated Hanford saltcake waste (for tanks AZ-101 and AY-102) were performed according to the test plan prepared by FIU-HCET. These studies correspond to Task 2 in the test plan. The tests have been aimed at gathering qualitative as well as quantitative information.

### 5.2.1 Experimental

Bench- and pilot-scale experimental setups were designed and assembled in FY 2000 (see Figs. 1 and 2). Both systems have a feed tank (with a heating system) and a Moyno pump (rotary progressing cavity type) for slurry transfer. The bench-scale setup contains a test section with a 3/8-in. inside diameter, and a 30-ft-long clear polyethylene flexible tube inside a transparent temperature-controlled bath. The pilot-scale experimental setup was designed and built to represent a part of the transfer system (from tank C-104 to tanks AZ-101 and AY-102) at the Hanford site. The design incorporated input from Hanford engineers and included a typical valve pit configuration (with several miter bends) and an incline section (2°) that represents the elevation difference between tanks. Transparent sections were included throughout the flow loop for plug monitoring. The inside diameter of the pipe is 1 in. for the clear PVC sections and the outside diameter is 1 in. for the stainless steel sections. Process conditions such as temperature (feed
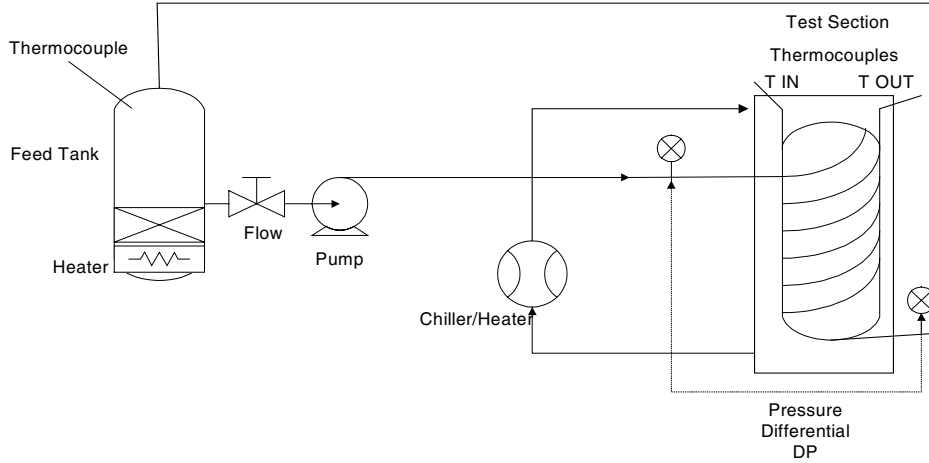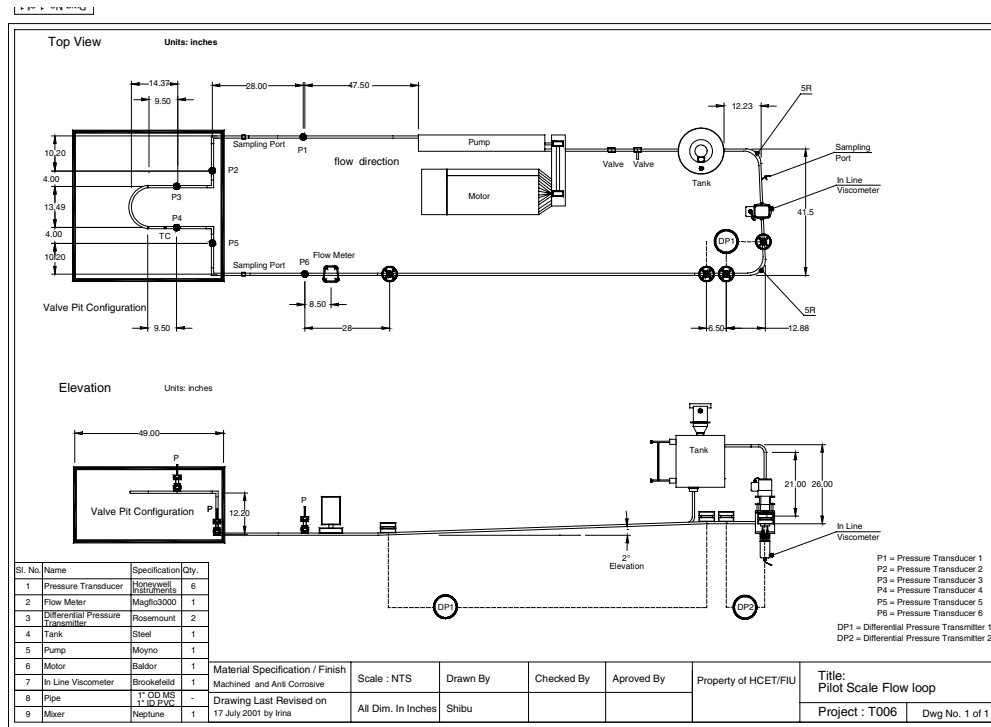
**Fig. 1. Schematic of the bench-scale unit.**



**Fig. 2. Layout of the pilot-scale unit.**

tank and test section) and flow rates were varied and pressure drop was measured and recorded in both systems using an automated data acquisition system (LabVIEW). A time-lapse video recorder system was utilized for plug formation and location. Plug sampling was performed through sampling ports located throughout the loops.

Two Hanford saltcake simulants (AZ-101 and AY-102) were developed and tested in both systems. The simulants' formulations, developed by ORNL, correspond to the best chemical inventory (without the radioactive components) available from the respective tanks. A test matrix was developed utilizing Hanford criteria for slurry transport. A temperature of 50°C (the Hanford criterion for minimum feed temperature) was maintained in the feed tank. The test section temperatures (15°C and 40°C) represented

conditions in the pipeline transfer. Different flow rates (laminar, critical, and turbulent regimes) were tested to understand the plug formation under various conditions, e.g., loss of flow or pump power, or partial plugging. PSD and rheology tests were performed with samples obtained at different times from the flow loop experiments.

### 5.2.2 Results and Discussion

**Pressure-drop bench-scale study**

Validation control tests were performed with water prior to testing the simulants in the flow loop. This task was performed to test the accuracy of the different pressure transducers present in the loop. Due to their larger density and viscosity, simulants showed higher pressure drops than water. This behavior, typical of non-Newtonian Bingham plastic fluids, is also true when the temperature is lower. Figures 3–6 show the pressure differential versus flow velocity correlation for the simulants (AY-102 and AZ-101) tested at two different test section temperatures (15°C and 40°C). Experimental and theoretical water pressure drops (control tests) are included on each figure for comparison.
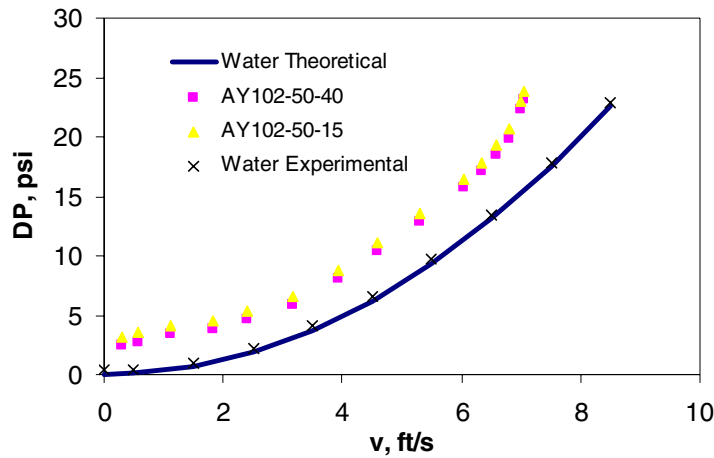


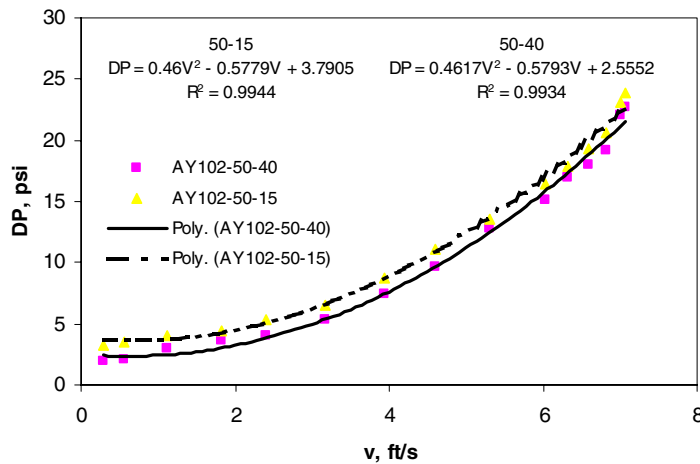**Fig. 3. Pressure drop versus flow velocity data for AY-102 simulant.**



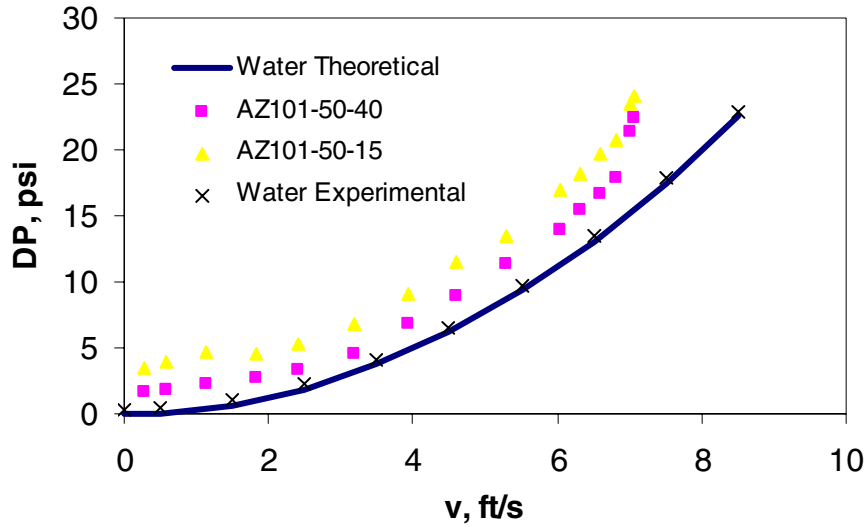**Fig. 4. Correlation models for AY-102 simulant pressure drop data.**

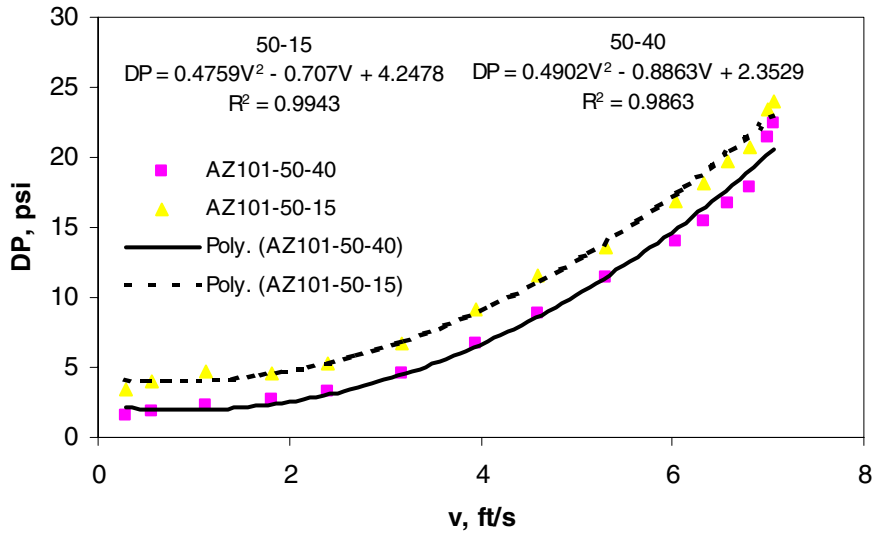**Fig. 5. Pressure drop versus flow velocity data for AZ-101 simulant.**



**Fig. 6. Correlation models for AZ-101 simulant pressure drop data.**

**Pressure-drop pilot-scale study**

Several pressure differential measurements were monitored during the pilot-scale study across different sections of the loop. Table 1 describes these measurements.

The validation and calibration of the pilot-scale loop was performed by running water tests through the system. The engineering Bernoulli equation for an incompressible fluid can be written as

$$\Delta P = (P_1 + \rho g z_1) - (P_2 + \rho g z_2) = K\rho \frac{V^2}{2} \tag{1}$$

**Table 1. Differential pressure measurements**

| Name | Pressure differential location | Pressure differential across |
|------|-------------------------------|------------------------------|
| DP1 | Valve pit configuration | One horizontal square bend |
| DP2 | Valve pit configuration | Two vertical bends<br>Upward flow direction |
| DP3 | Valve pit configuration | Horizontal 5-in. radius 180° bend |
| DP4 | Valve pit configuration | Two vertical bends<br>Downward flow direction |
| DP5 | Valve pit configuration | One horizontal square bend |
| DP6 | Incline section after valve pit | 7-ft incline section |
| DP7 | Feed tank return | Horizontal 5-in. radius bend |

where

ΔP is the differential pressure between points 1 and 2,

K is the *velocity head loss coefficient*,

V is the reference velocity.

In Fig. 7, the *K* values for the AZ-101 and AY-102 tests at different temperatures and water are compared. As expected, the velocity head loss is more for the simulants than for water at all locations. The higher pressure losses can be attributed to the higher density and viscosity of AZ-101 and AY-102 simulants in the loop. The simulant AZ-101 shows the highest pressure drop at all locations but DP4. The effect of temperature is not very pronounced.
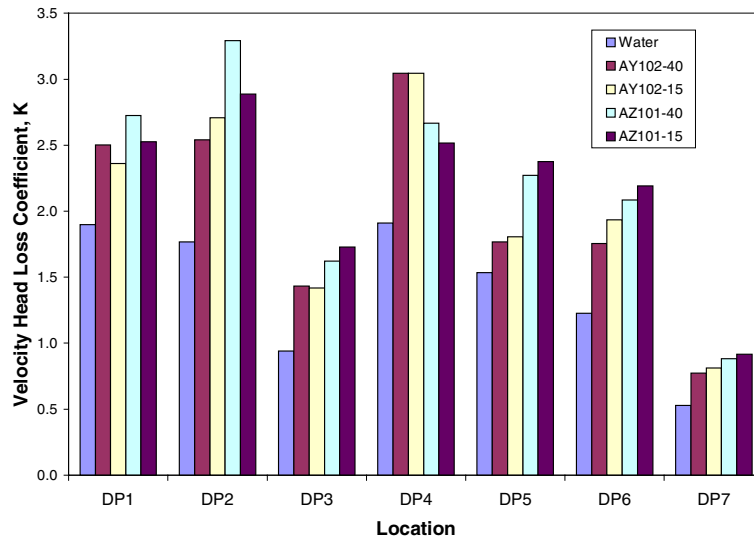


**Fig. 7. Comparative plot of the K-values for the various locations in the loop.**

The velocity head loss values reported in literature (Perry, Green, and Maloney 1997) for a 90° bend and 180° bend are somewhat smaller, as shown in Table 2.

*K* values can be calculated in the same manner at the site to determine head losses in bends and pipe sections where plugging might occur. Details of these calculations can be found in Ebadian, López, and Srivastava 2002.

**Table 2. Bends head loss values**

| Fitting | K | |
|---|---|---|
| | Experimental-water | Literature |
| 180° 5-radius bend | 1.7 | 1.5 |
| 90° bend | 0.5 | 0.75 |

**Simulant characterization**

1. Rheology measurements of the simulants (AY-102 and AZ-101) were carried out by using a Haake RS75 RheoStress instrument. These measurements were done at different temperatures. A Bingham plastic model was observed in all cases. The Bingham model equation is $\tau = \tau_o + \gamma\eta$ where $\tau$ = shear stress, $\tau_o$ = yield stress, $\gamma$ = shear rate, $\eta$ = consistency.

Bingham plastic behavior was observed in the simulants because of the solids concentration (about 20% by volume). This rheologic behavior is consistent with Hanford waste. Therefore we can say the tested simulants represented the Hanford waste's physical and rheologic properties (Tables 3 and 4).

**Table 3. Summary of simulant AY-102 rheology**

| Temperature, $^o$C | Consistency, $N.s/m^2$ | Yield stress, Pa |
|---|---|---|
| 15 | 0.0154 | 1.227 |
| 25 | 0.0153 | 0.9751 |
| 30 | 0.0132 | 0.7391 |
| 40 | 0.0123 | 0.6975 |
| 45 | 0.0116 | 0.6169 |
| 50 | 0.0112 | 0.6097 |

**Table 4. Summary of simulant AZ-101 rheology**

| Temperature, $^o$C | Consistency, $N.s/m^2$ | Yield stress, Pa |
|---|---|---|
| 15 | 0.0135 | 0.8431 |
| 25 | 0.0125 | 0.7197 |
| 30 | 0.0117 | 0.6523 |
| 40 | 0.0103 | 0.5395 |
| 45 | 0.0097 | 0.5118 |
| 50 | 0.0092 | 0.5091 |

2. PSD measurements were performed using scanning electron microscope pictures of dry particles (see Fig. 8). These particles were obtained from samples taken at different times during the experimental runs from both the bench- and pilot-scale studies. An image processing and analysis software (IMAQ Vision Builder) was used to analyze the pictures. This software performs automated particle analysis and can be used to measure characteristics such as particle diameter, area, mean, centroid, and perimeter, of user-defined regions of interest. Figure 8 shows a panoramic view of simulant particles. Individual pictures are taken from this picture at higher magnification to use in the analysis.

Table 5 and Fig. 9 show the results of the PSD analysis of this sample (AY-102 simulant), where a particle mean size of 94 µm was obtained.
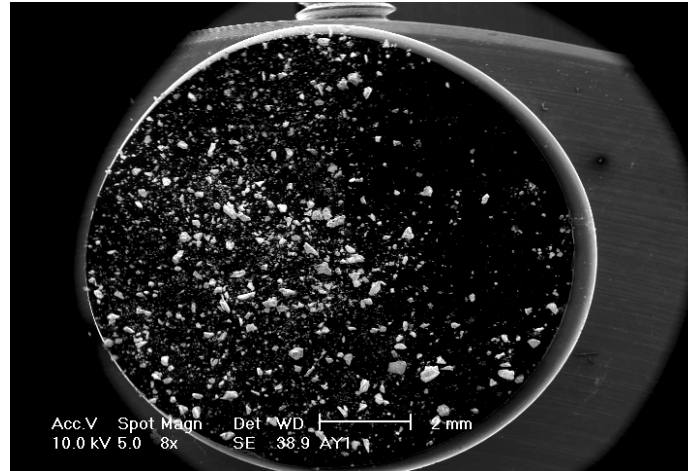
**Fig. 8. Scanning electron microscope picture of an AY-102 sample.**

**Table 5. Particle size distribution of an AY-102 sample**

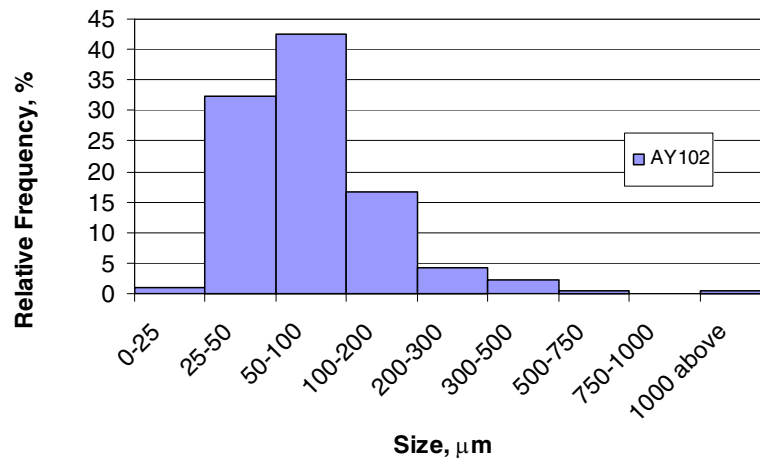| Size, µm | Cum. frequency | Frequency | Rel. frequency, % |
|---|---|---|---|
| 25 | 39 | 39 | 0.98 |
| 50 | 1321 | 1282 | 32.35 |
| 100 | 3010 | 1689 | 42.62 |
| 200 | 3675 | 665 | 16.78 |
| 300 | 3846 | 171 | 4.31 |
| 500 | 3931 | 85 | 2.14 |
| 750 | 3946 | 15 | 0.38 |
| 1000 | 3947 | 1 | 0.03 |
| Above 1000 | 3963 | 16 | 0.40 |



**Fig. 9. Particle size distribution of an AY-102 sample.**

Data obtained in the PSD analyses relate to Jewett and Jensen (2000) findings, as most samples had a mean particle size ranging from 90 to 150 µm. All results can be found in our FY 2001 year-end report (Ebadian, López, and Srivastava 2002).

**Study of kinetics of particle growth**

Pipeline plugging at the DOE sites is caused mainly by solids formation (crystal growth) during supernatant and slurry transfer. This phenomenon is caused by temperature drop due to heat loss in the transfer lines. The objective of this study was to understand and delineate the kinetics of solids formation in a batch (static) and a flow (dynamic) system. Batch and flow experiments were performed with a simple three-species chemical system (hydroxide-phosphate-fluoride) to determine how much and how fast solids form under different conditions.

**Batch tests.** Batch tests were performed in a beaker to determine the kinetics of crystal growth and nucleation. Crystal growth occurs when the size of a single crystal/particle increases. Nucleation refers to crystal/particle population (number of particles). The purpose of these tests was to measure how fast and how many crystals formed at a given temperature. The simulant used was a hydroxide-phosphate-fluoride system (referred to as X1). The composition of this simulant was $3M$ $NaOH + Na_3PO_4.12H_2O + 0.2M$ $NaF$. The measured density and viscosity of this simulant at room temperature ($25°C$) were 1.16 g/ml and 13 cP, respectively. The batch test matrix is summarized in Table 6 and the test results are presented in Tables 7–11 and Figs. 10–12.

**Table 6. Test matrix for batch tests**

| Temperature (°C) | Time (min) |
|---|---|
| 80, 50, 30, 25, 15 | 0, 5, 10, 15, 20, 30, 60 |

**Table 7. Crystal growth data for the batch-scale study ($80^oC$)**

| Temperature (°C) | Time (min) | Solids (wt%) | Crystals (in.$^2$) | Mean size (μm) |
|---|---|---|---|---|
| 80 | 0 | 0.00180 | 158 | 128 |
| 80 | 5 | 0.00170 | 168 | 156 |
| 80 | 10 | 0.00170 | 231 | 157 |
| 80 | 15 | 0.00180 | 297 | 173 |
| 80 | 20 | 0.00175 | 338 | 176 |
| 80 | 30 | 0.00170 | 384 | 212 |
| 80 | 60 | 0.00165 | 429 | 212 |

**Table 8. Crystal growth data for the batch-scale study ($50^oC$)**

| Temperature (°C) | Time (min) | Solids (wt%) | Crystals (in.$^2$) | Mean size (μm) |
|---|---|---|---|---|
| 50 | 0 | 0.0189 | 451 | 225 |
| 50 | 5 | 0.0190 | 474 | 225 |
| 50 | 10 | 0.0210 | 499 | 240 |
| 50 | 15 | 0.0230 | 524 | 248 |
| 50 | 20 | 0.0250 | 537 | 263 |
| 50 | 30 | 0.0263 | 546 | 265 |
| 50 | 60 | 0.0343 | 568 | 278 |

**Table 9. Crystal growth data for the batch-scale study (30°C)**

| Temperature (°C) | Time (min) | Solids (wt%) | Crystals (in.$^2$) | Mean size (µm) |
|---|---|---|---|---|
| 30 | 0 | 0.109 | 607 | 295 |
| 30 | 5 | 0.112 | 669 | 300 |
| 30 | 10 | 0.119 | 701 | 302 |
| 30 | 15 | 0.13 | 725 | 315 |
| 30 | 20 | 0.145 | 802 | 321 |
| 30 | 30 | 0.1524 | 845 | 340 |
| 30 | 60 | 0.1567 | 874 | 356 |

**Table 10. Crystal growth data for the batch-scale study (25°C)**

| Temperature (°C) | Time (min) | Solids (wt%) | Crystals (in.$^2$) | Mean size (µm) |
|---|---|---|---|---|
| 25 | 0 | 0.175 | 890 | 385 |
| 25 | 5 | 0.1810 | 892 | 401 |
| 25 | 10 | 0.1880 | 935 | 415 |
| 25 | 15 | 0.1920 | 952 | 425 |
| 25 | 20 | 0.1960 | 966 | 463 |
| 25 | 30 | 0.2053 | 988 | 504 |
| 25 | 60 | 0.2132 | 990 | 555 |

**Table 11. Crystal growth data for the batch-scale study (15°C)**

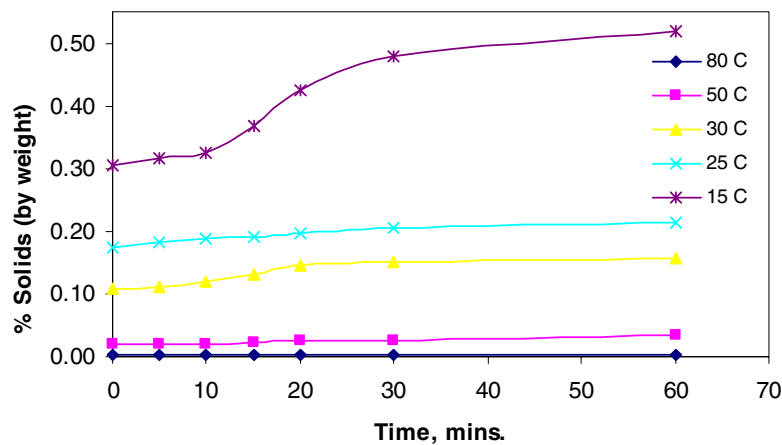| Temperature (°C) | Time (min) | Solids (wt%) | Crystals (in.$^2$) | Mean size (µm) |
|---|---|---|---|---|
| 15 | 0 | 0.3055 | 1025 | 600 |
| 15 | 5 | 0.3153 | 1145 | 609 |
| 15 | 10 | 0.3244 | 1356 | 850 |
| 15 | 15 | 0.3670 | 1478 | 1520 |
| 15 | 20 | 0.4250 | 1630 | 1780 |
| 15 | 30 | 0.4790 | 1700 | 2005 |
| 15 | 60 | 0.5195 | 1774 | 2150 |



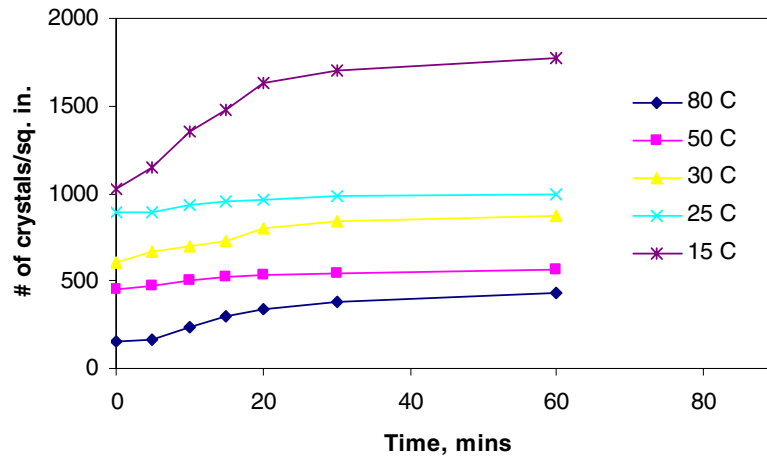**Fig. 10. Effect of temperature on solids concentration.**

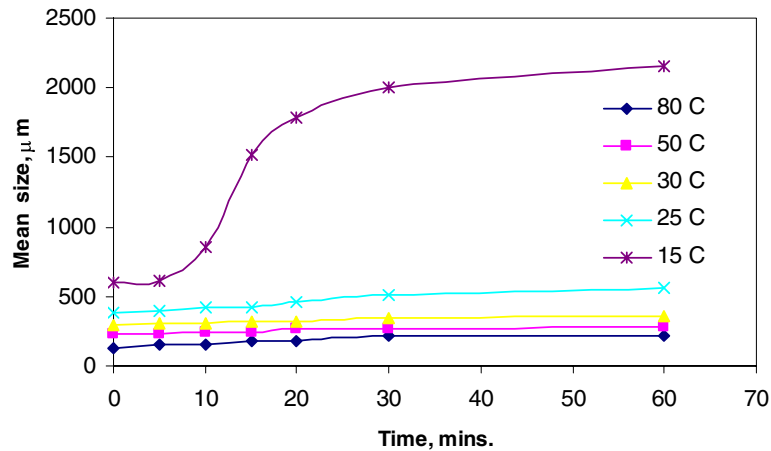**Fig. 11. Effect of temperature on number of particles.**



**Fig. 12. Effect of temperature on particle mean size.**

As observed in the tables and charts, temperature played an important role in these tests. At lower temperatures, the sizes and the number of particles increased considerably.

**Flow experiments**

Flow experiments were performed in the pilot-scale flow loop (shown in Fig. 2) to determine the kinetics of solids formation in a flow system. The simulant (X1) was prepared in a fume hood and transferred to the feed tank (see Sect. 2.1). The simulant was pumped at low (2.5 ft/s), middle (5 ft/s), and high (7.5 ft/s) flow velocities. The temperature in the tank was maintained at 50°C, and the temperature at the test section was varied from 50 to 10°C. Samples were taken from two sampling ports located before and after the test section (IN and OUT). Similarly to the batch tests, samples were filtered for particle solids concentration determination and size distribution analyses. In addition, power outage was simulated by turning the pump off and leaving the simulant in the system for a long period of time (12+ hours). The pipeline got plugged with this exercise. Crystals were observed through the clear section of the loop. Unplugging was attained by heating the system at 50°C and by turning the pump back on.

**Table 12. Test matrix for flow experiments**

| Feed tank temperatures (°C) | Test section temperatures (°C) | Flow velocity (ft/s)* |
|---|---|---|
| 50 | 15, 25, 40, 50 | 2.5 |
| 50 | 15, 25, 40, 50 | 5.0 |
| 50 | 15, 25, 40, 50 | 7.5 |

*The diameter of the pipe is 1 in.

**Table 13. Qualitative experimental observations**

| Simulant | Feed tank temperature (°C) | Flow* velocity (ft/s) | Temperature at the test section (°C) | | |
|---|---|---|---|---|---|
| | | | 15 | 25 | 45 |
| X1 (3M NaOH + 0.2M NaF + 0.6M Na$_3$PO$_4$) | 50 | 2.5 | Considerable solids formation<br><br>Plugging observed mainly at bends<br><br>Settled bed<br><br>Abnormal flow conditions | Solids formation observed<br><br>No plugging<br><br>Normal flow conditions | No precipitation observed<br><br>Normal flow conditions. |
| | 50 | 5.0 | Solids formation at a faster rate<br><br>Moving bed forming partial plugging<br><br>Partial plugging<br><br>Poor flow conditions | Few solids observed increasing at a slight faster rate<br><br>Normal flow conditions | No precipitation observed<br><br>Normal flow conditions. |
| | 50 | 7.5 | Solids formation observed<br><br>Normal flow conditions | Few solids observed<br><br>Normal flow conditions | No precipitation observed<br><br>Normal flow conditions |

*Pipe outer diameter = 1 in.

Quantitative results and data correlation from this study can be found in Ebadian, López, and Srivastava (2002).

**Pressure drop across a bend**

The objective of this test was to collect and correlate pressure drop data across a single bend typical of a Hanford connector for a simulated waste slurry flow system. A physical simulant (sand-and-water slurry) was selected for the tests. James Jewett of Numatec Hanford Corporation mentioned that the site engineers use e**quivalent length or velocity** correlations for calculating pressure drop across a bend. These correlations were developed for homogeneous flow, and their applicability to the heterogeneous system had not been looked into. One of the important factors that affects pressure drop is the amount of solids loading by volume (Cv). A physical simulant refers to one with physical properties similar to those of the actual waste, whereas a chemical simulant refers to one with similar chemical content. The use of a physical simulant was included in the test plan for FY 2001 to perform some tests using one of the same simulants that have been or will be used in the horizontal (TFA-retrieval) pipeline flow loop. The PSD and median of the selected slurry (mixture) was based on Rosin-Rammler distributions. The Rosin-Rammler function is widely used in PSD characterization. It is a two-parameter function ($n$ and $x_R$) given as a cumulative percentage retained, and it is expressed as (Allen 1997, p. 88):

$$R = 100 \exp\left[-\left(x/x_R\right)^n\right]$$

where
$R$ = weight of percentage retained,
$x$ = particle size,
$n$ = spread of the distribution,
$x_R$ = fineness of the material.

Figure 13 shows a comparison of Rosin-Rammler distributions. It includes median particle sizes of 50, 100, and 250 μm with $n$ values of 1.7, 4, and 7.
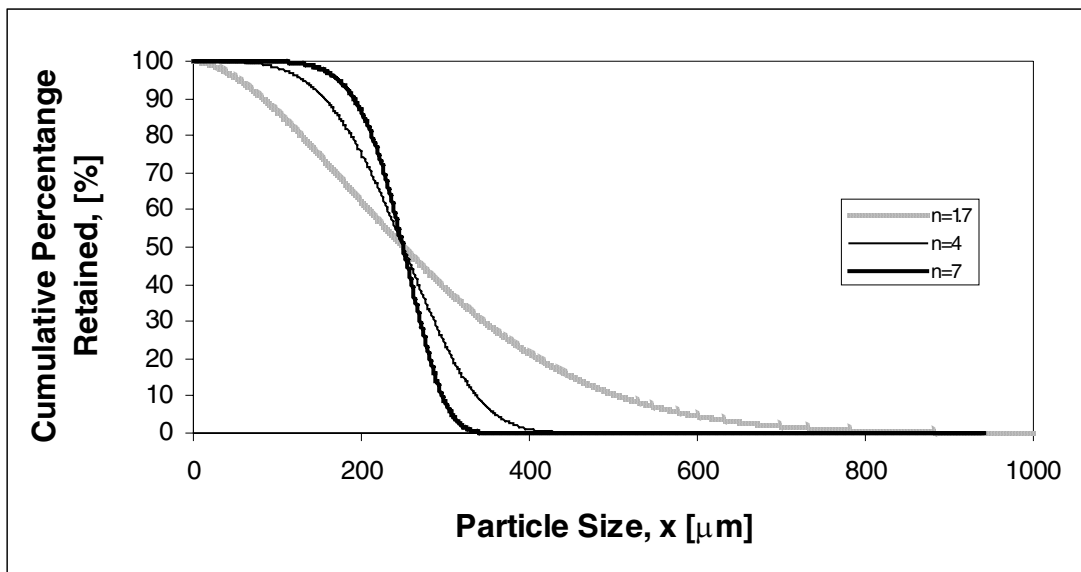


**Fig. 13. Rosin-Rammler distributions with parameter "$n$"= 1.7, 4, and 7 at median size of 250 μm.**

The flow loop (Fig. 2)—initially designed to map the chemical, thermal, and flow regimes that define the boundary between acceptable and unacceptable waste transport operations—was modified to perform pressure drop measurements across a sharp 90° bend (Fig. 14). It includes two straight pipe sections (6 and 5 ft) before and after a 90° bend bypassing the valve pit configuration. Lengths were based on standard L/D values (60) for turbulent flow.

Figure 15 shows the 90° bend section. The pressure differential is measured in the straight sections before and after the loop as well as across the bend. Figure 16 is an overview of the modified section of the flow loop.
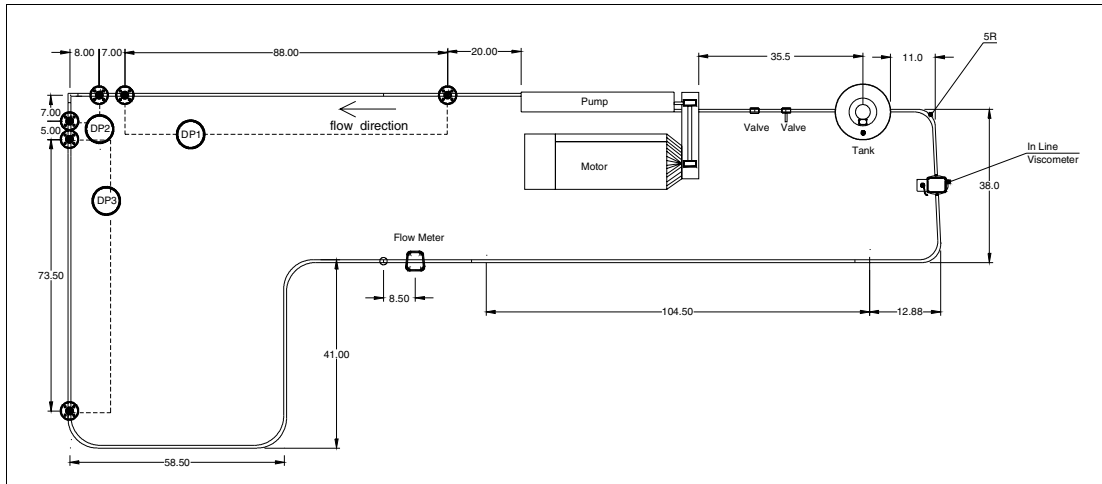


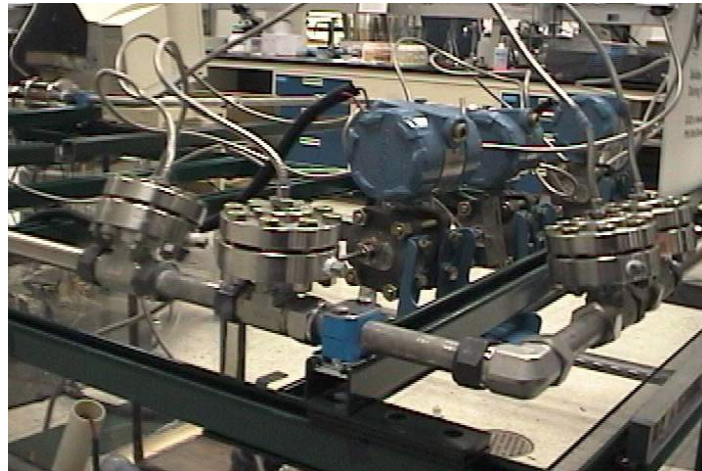**Fig. 14. Layout of the modified flow loop.**



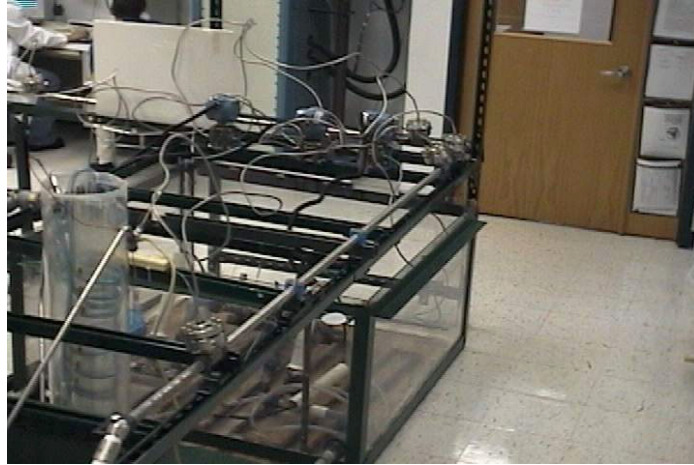**Fig. 15. The 90° bend in the flow loop.**

**Fig. 16. Overview of the modified flow loop.**

**The Wasp model**

Wasp et al. (1978) developed an empirical method for calculating the pressure gradient as the sum of the gradients due to the symmetrically suspended material and to the asymmetrically suspended and sliding material. Wasp et al. pointed out that with a reasonable range of particle sizes present in a slurry, the smallest particles will normally be in the symmetric concentration flow pattern; the intermediate and large particles will be in the asymmetric pattern; and the largest may slide on the bottom of a pipe. Wasp's method provides a systematic means of interpolating between the two flow pattern extremes of homogeneous flow and asymmetric suspension and sliding bed flow, thus obtaining the results for usual mixed-size slurries. The work of Wasp et al. is of great practical significance since it is based on, and confirmed by, extensive tests on large-diameter commercial pipelines transporting coal-water slurries. To apply Wasp, the physical properties data for our slurry were adapted to fit the model. The weighted average method was used to calculate the average density of solids in the slurry and average densities of particles in different size ranges. Results of this study can be found in Ebadian, López, and Srivastava (2002).

**Study of unplugging methods**

The main objective of this study was to focus on methods than can be used to unplug a line after it has plugged. The system under consideration was a simple, one-specie sodium phosphate. This system was chosen because sodium phosphate crystals have been observed in various studies conducted on Hanford simulants. $CO_2$ was bubbled into this plug, and solids concentration was determined before and after this exercise. The variables of interest were concentration of the mother solution, the age of the solids or crystals formed, and the rate of application of the unplugging agent. The ability of $CO_2$ to unplug the system was studied. Even though results showed that solids concentration did not vary considerably after bubbling $CO_2$, this study should be conducted in a flow system and with different plugs to mimic Hanford plugged lines and conditions. Results of this preliminary test can be found in Ebadian, López, and Srivastava (2002).

**5.3 Conclusion**

Flow experiments with Hanford simulants AY-102 and AZ-101 did not produce pipeline plugging even under the worst flowing conditions. This is mainly because these simulants contain no more than 20% of solids by volume, and the chemical contents are mostly insoluble solids with no saltcake. These wastes behave like diluted sludge rather than saltcake waste. The Bingham plastic rheologic behavior is typical

of a non-Newtonian fluid. Low temperatures contribute considerably to particle growth. Heat-tracing the pipelines may help to avoid plugging. Further investigation will be conducted in FY 2002 to analyze whether chemical unplugging might be viable at the site.

## 5.4 References

Allen, T., 1997. *Particle Size Measurement*, 5th ed., Vol. 1, Chapman and Hall, New York.

Ebadian, M. A, R. D. López, and R. Srivastava 2002. *Solids Formation And Feed Stability During Waste Slurry Transfer: Fiscal Year 2001 Year-End Report*, HCET-2000-T006-003-30, Hemispheric Center for Environmental Technology, Florida International University, Miami (January).

Jewett, J. R., and L. Jensen 2000. *Assessment of Available Particle Size Data to Support an Analysis of the Waste Feed Delivery Transfer System*, RPP-6247, Rev. 0, CH2MHill Hanford Group, Richland, Washington (August).

Perry, R. H., D. W. Green, and J. O. Maloney 1997. *Perry's Chemical Engineers' Handbook*, 7th ed., McGraw-Hill, New York.

Srivastava, R., and R. D. López 2000. *Solids Formation and Feed Stability Testing During Waste Slurry Transfer: Test Plan for FY 2000*,  HCET-1999-T006-001-02 Rev.3, Hemispheric Center for Environmental Technology, Florida International University, Miami (January).

Wasp, E. J., J. P. Kenny, and R. L. Gandhi 1978. *Solid-Liquid Flow Slurry Pipeline Transportation*, Gulf Publishing Company, Houston.

# 6. TRANSPORT STUDIES ON INTERIM STABILIZATION OF SUPERNATANT STREAMS: DIAL/MSU FY 2001 SUMMARY PROGRESS REPORT

J. S. Lindner, Vijay Raju, Tushar Durve, R. K. Toghiani, and H. Al Habbash

*Diagnostic Instrumentation and Analysis Laboratory*
*Mississippi State University*
*205 Research Blvd.*
*Starkville, MS, 39759*

## Abstract

Previous salt well liquor transfers from tank 241-SX-104 at the Department of Energy's Hanford site have resulted in the formation of pipeline plugs that lead to delays in site processing schedules. To evaluate the processes associated with the movement of high-ionic-strength brines, a laboratory-scale flow loop was designed and constructed; and experiments were conducted using surrogates representative of the tank and diluted wastes. The effects of flow velocity, heat transfer, and phosphate concentration were evaluated. Imaging experiments were employed to ascertain the growth of the particles and subsequent aggregates, and the formation of the plug. Particles were observed to grow at rates of up to 2 $mm^2$/s; a maximum average aggregate growth rate of 19 $mm^2$/s was found. Sedimentation of the particles and the agglomerates was well described by the equation developed by Durand (1952). Models for the increase in pressure as the particles sediment, and for the unsteady state heat transfer associated with the process, have been compared with the experimental results. The data are represented in terms of an operating envelope that can be used by facility engineers to ascertain the waste dilution required to avoid a plug for a given temperature or heat flux.

## 6.1 Introduction

Tank farm operations at the Department of Energy's Hanford site include the interim stabilization program through which the supernatant and interstitial liquor in the single-shell tanks are transferred to one of the double-shell tanks and then to an evaporator (Fluor Daniel Hanford 1998). The process was developed to minimize waste and to reduce the likelihood of leakage. Supernatant and interstitial liquids percolate through the waste to a screen at the base of an inserted dual pump assembly located in the lower portion of the tank. The liquid is then pumped out of the tank to the piping network. Process flow rates are dependent on the infusion rate of supernatant into the salt well and are laminar (0.4 to 5 gal/min through nominal 3-in. mild steel pipe). Many portions of the transfer lines are heat-traced; however, junction boxes used for routing are configured with either rigid or flexible insertion pipes or jumpers and are contained in concrete bunkers.

A number of the aqueous components in the supernatant are close to saturation; consequently, difficulties have arisen with regard to formation of unwanted solids. Recently, plugs developed during stabilization of tanks 241-SX-104 and 241-U-103 (Reynolds 2000). The primary solid responsible has been tentatively identified, through laboratory screening experiments, as sodium phosphate dodecahydrate, $Na_3PO_4 \cdot 12H_2O$ (Herting 1998; Steen 1999). Supernatant phosphate concentrations of as low as 0.044 *M* were shown to result in crystallization (gel formation) at a temperature of 25°C.

Changes in waste temperature will affect flow properties through changes in the solid–liquid equilibria. Possible ways to overcome unwanted solids formation include maintaining the supernatant at temperatures above the freezing point of the solids or diluting the waste. Provisions for the addition of diluent (water) are incorporated in the salt well pump design; however, it is difficult for facility operators to know, a priori, the amount of water necessary to maintain the supernatant below the saturation level (Reynolds 2000). Factors such as compositional heterogeneity within a given tank and the expense of core sampling and analysis imply that variations in the chemical composition of the liquid should be expected and are likely significant. Furthermore, adding large amounts of water exacerbates storage limitations.

The development of a plug results in lost time and, in some cases, the inability to use a specific transfer route. Plug remediation has focused on physical methods such as the use of pressure and/or steam injection (Reynolds 2000). Only marginal success has been attained. Other physical and chemical methods may be suitable; in order to understand the processes needed to unblock an obstruction, information is required on the processes leading to development of a plug.

## 6.2 Experimental Section

An initial surrogate recipe for the composition of the supernatant from Hanford tank 241-SX-104 was developed by R. Hunt at Oak Ridge National Laboratory and was based on the previously cited work performed at Hanford and the best basis inventory (Hunt 2000). The surrogate consisted of water and the sodium salts of aluminate, nitrate, hydroxide, carbonate, and phosphate in mole fractions of 0.0153, 0.106, 0.03, 0.0061, and 0.003, respectively. Screening experiments revealed that an isotropic clear solution was present at a temperature of 50°C and that both loose solids and the sodium phosphate dodecahydrate "needle" crystals were formed at 40°C. The recipe was then altered by varying the carbonate and the phosphate contributions so that only the sodium phosphate structure was obtained. In this way, the formation of a plug due only to the phosphate particles could be studied. The revised carbonate and phosphate mole fractions were.0.0015 and 0.0045, respectively. This solution was clear at 50°C, and only phosphate crystals were observed at temperatures of down to 25°C. An image from the polarized light microscope (PLM) is given in Fig. 1. The molar phosphate concentration for this sample was determined as 0.22.
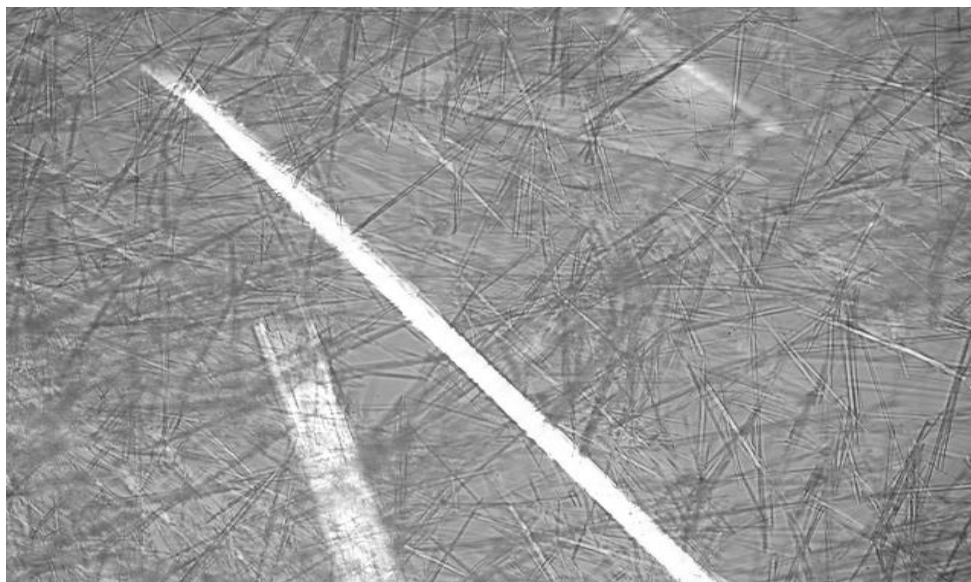


**Fig. 1. Polarizing light microscope image of the sample 8 surrogate.** The cylinders observed in the image are $Na_3PO_4 \cdot 12H_2O \cdot 0.25NaOH$.

The PLM results are consistent with the solids observed from the actual SX-104 supernatant sample (Steen 1999). The main difference between the actual waste and the surrogate was the temperatures at which the phosphate solids were observed, 23 and 40°C, respectively. Other solids associated with the compositions included sodium nitrate and gibbsite (Al(OH)$_3$). Sodium nitrate was seen at 25°C. The Environmental Simulation Program (ESP) predicted this solid, along with gibbsite (which was not observed in any of the PLM images). At temperatures above 41°C, the only solid predicted by ESP was sodium phosphate octahydrate. Attempts to observe the corresponding crystal with the PLM were unsuccessful. The particle size is apparently smaller than the dimension observable with the highest effective magnification (400×) of the current instrument configuration. At an approximate temperature of 40°C, the model calculations predict a transition to the dodecahydrate form, which comprises 100% of the solids in the system at that temperature. The overall stream density increases with a decrease in temperature owing to the additional partitioning into the solid phase. Of interest in the model predictions are the relatively small values of the percentages of solids by weight and volume. Full details are available in Lindner et al. (2000).

Development of the laboratory-scale test loop has been described previously and was based on the Reynolds numbers encountered during the Hanford transfers (Lindner, Habbash, and Taghiani 2000). A diagram of the flow loop is shown in Fig. 2. The thermocouples, the stainless steel channel, the pressure transducers, and the surrogate/hot water flow meters were selected to minimize corrosion. The thermocouples and pressure transducers were interfaced to a data acquisition system, and pressure drops and temperatures were logged at 1-s intervals. A booster pump, not shown, was used to increase the delivery of water from the tap. The temperature in the test section of the flow loop was controlled by four heat exchangers. Water flow rates of from 0.3 to 1.6 gpm, selectable for each exchanger, could be obtained. Shutting off three of the exchangers allowed a flow rate of as high as 3 gpm through the remaining shell. The design included provisions for recycling the surrogate sample to the inlet tank prior to the solution's entering the channel (for continuous mixing and surrogate conservation in the case of a plug) and at the end of the channel for runs at higher Reynolds numbers. In the event of plug formation, the sample line could be drained at an appropriate sample port, and hot water could be added at the pump head in an attempt to unblock the channel.
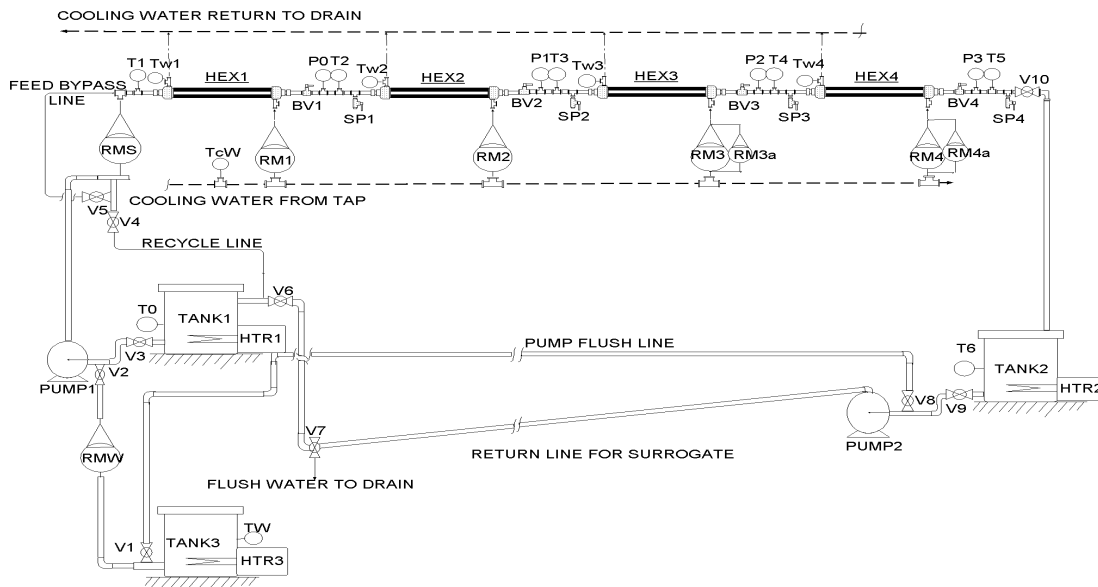


**Fig. 2. Diagram of the laboratory-scale salt well pumping flow loop.** Designations are P, pressure transducer; T, thermocouple; F, flow meter; IH, immersion heater; S, sampling port. Dashed lines correspond to the flow of the cooling water. Surrogate flows from left to right.

Most of the experimental results presented in Sect. 6.3 were obtained when the channel downstream of the second heat exchanger was replaced with a Plexiglass tube. No differences were observed in the pressure increase, temperature decrease, or time to achieve a plug, whether the clear channel or the original channel was used. The clear channel permitted an assessment of the particle dynamics. For this purpose, a small black and white camera ($640 \times 480$ pixels) equipped with a 75-mm focal lens, which was doubled to an effective focal length of 150 mm, was used to collect images of particle and agglomerate growth and bed area fractions during selected experiments. The camera interfaced with a personal computer through a frame-grabbing board. Software was written in-house for control of the image collection frequency and for the storage of the raw images on the permanent disk of the computer. Images were originally collected at a rate of 12.5 frames per second and stored in bitmap format. Analysis was performed using the software associated with the PLM. Initially the images were converted to an 8-bit gray-scale representation, cropped to the channel dimensions, contrast-enhanced, and then stored in the jpeg format.

Measurements were confined to an approximate 2-in. length of the channel 19 in. downstream of heat exchanger number 2. A scale was placed over the observation area to provide a means for direct calibration. The lens combination corresponded to a spatial resolution of 13.1 pixels/1000 microns or about 1 pixel = 80 microns.

The frame collection rate of the camera was sufficient to allow tracking of the individual particles and agglomerates, thus allowing for the determination of particle or agglomerate velocities. Bed formation occurred following single particle growth and then agglomeration. The bed area was determined by manual tracing of the bed with the tool supplied with the software, followed by integration. This area was then compared with the total area within the probe volume of the channel.

In all experiments, water at 50°C (contained in tank 2, Fig. 2) was used to preheat the channel; there was no water flow to the heat exchangers. Once a stream temperature of 50°C was attained, the channel was drained and a small amount of surrogate was allowed to flow without recycle. The surrogate was then admitted to the channel and the flow rate set to the desired value. The stream was then allowed to passively cool to a temperature between 46 and 47°C. The chosen heat exchanger(s) were then activated at the selected cooling water flow rate. Flow stream temperatures and pressures were recorded until plug formation occurred. Process data were then transferred to a spreadsheet file, which was analyzed for global parameters, such as the stream cooling rate, the temperature upon plug formation, and the time necessary for a plug to form.

The initial experiments centered on the analysis of phosphate plug formation in the base composition (0.22 $M$ PO$_4$) as a function of the axial velocity or flow rate of the surrogate. Thereafter, experiments were performed at different cooling rates. Finally, some limited experiments were carried out at various phosphate loadings.

## 6.3 Results And Discussion

### Surrogate Flow Experiments at a Reynolds Number of 235

Figure 3 depicts the temperatures and pressures recorded for an experiment with a surrogate flow rate of 3.5 gal/h (Reynolds number of 235) and a cooling water flow rate of 0.5 gal/min to heat exchanger number 2 (Fig. 2). The plot has been confined to the time at which the heat exchanger was activated and a complete plug was formed. The tank temperature, as well as the temperatures upstream of the heat exchanger, remained constant. The temperature downstream of the heat exchanger decreased, gradually approaching 39–40°C. The upstream pressure remained constant to 150 s and thereafter increased until a
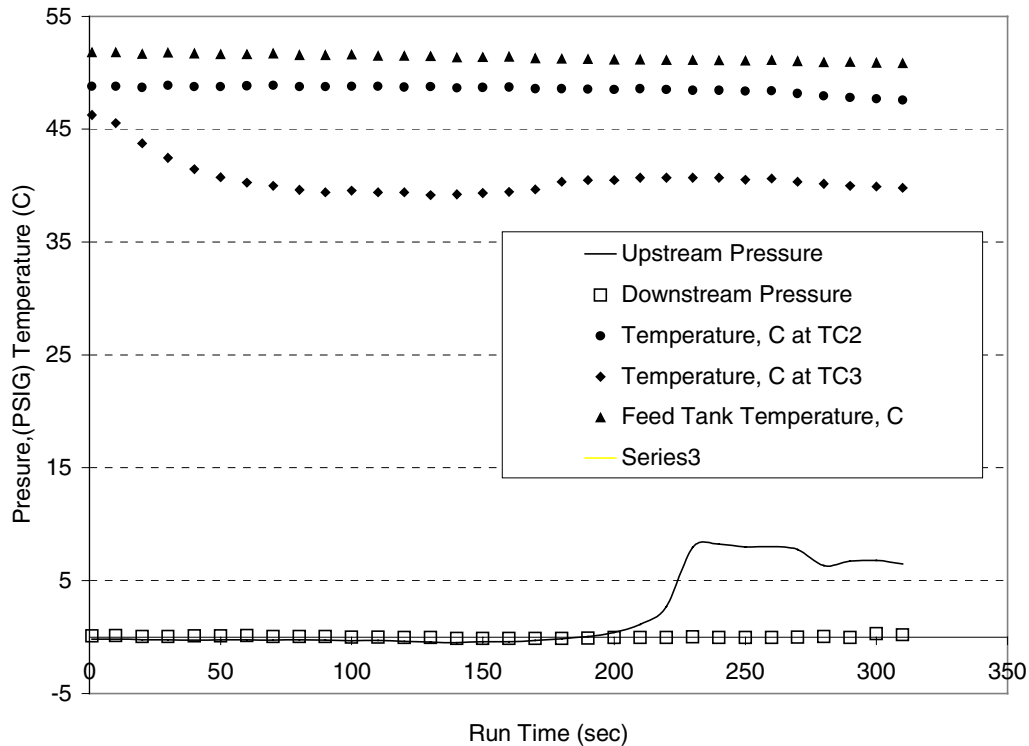
**Fig. 3. Temperatures and pressures recorded for an experiment with a Reynolds number of 235.** (See Fig. 2 for location of temperature and pressure sensors.)

maximum value was attained, indicating plug formation and corresponding to the pressure head on the pump. The downstream pressure remained low, indicating that plug formation occurred within the channel. All of the processes leading to the formation of the plug took less than 4 minutes.

Images were collected at a location 20 in. downstream from the second heat exchanger, from approximately 150 s after the cooling water was supplied until plug formation was complete. Initial precursor events are thought to have commenced before the start of frame collection; however, the dimensions of any particles present prior to 150 s were smaller than the minimum resolution of the imaging system. Representative frames for the growth and transport of a small particle observed at a time of 208.72 s are shown in Fig. 4. In the first frame, the particle lies above the 19 7/8-in. mark on the scale and exhibits a rod-like shape. The second frame, taken directly after the first, shows the movement of the particle and also indicates growth.

Similar images were collected showing the growth and deposition behavior of the aggregates and the development of the bed. Data on the width, length, and velocities of the particles and the aggregates were tabulated. Average axial ratios and the ultimate sizes that particles or agglomerates attained before exiting the viewing or probe area were determined. Examples of particle growth are collected in Fig. 5.

The ultimate size of the single particles did not change significantly as the bed formation proceeded. The plot indicates the presence of single particles and depositing particles until about 213 s after application of the heat exchanger, at which time agglomerate formation began to dominate. Some single particles were still observed after 213 s; however, the images primarily showed agglomerate formation, deposition, and further bed development. Calculated velocities were found to decrease as the run progressed, consistent with the increase in pressure (arising from the accumulation and transport of solids) observed from the upstream transducer (Fig. 3).
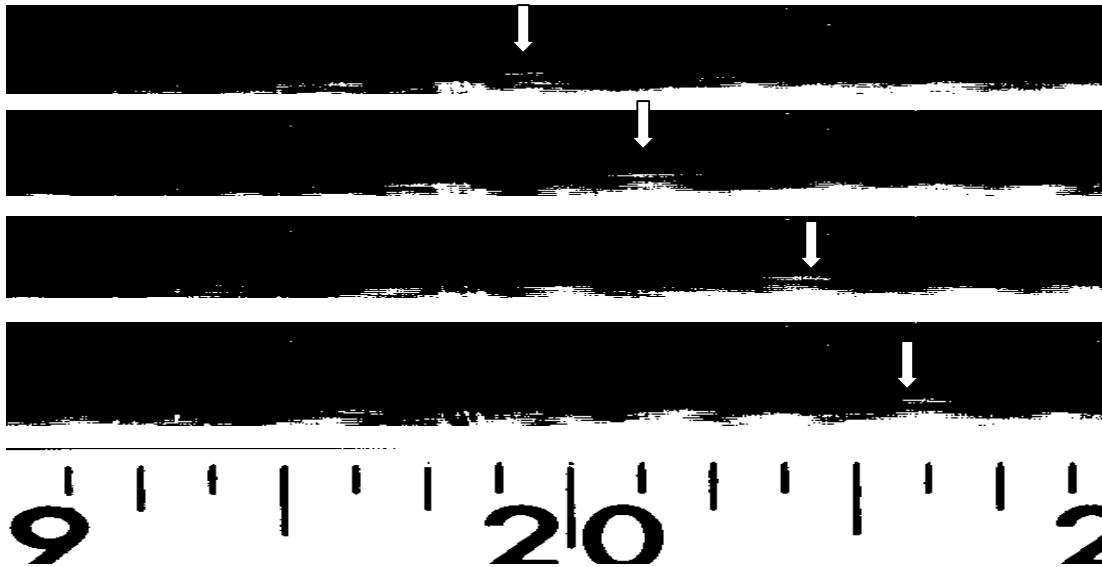
**Fig. 4. Representative images for a single particle observed during the experiment at a Reynolds number of 235.**
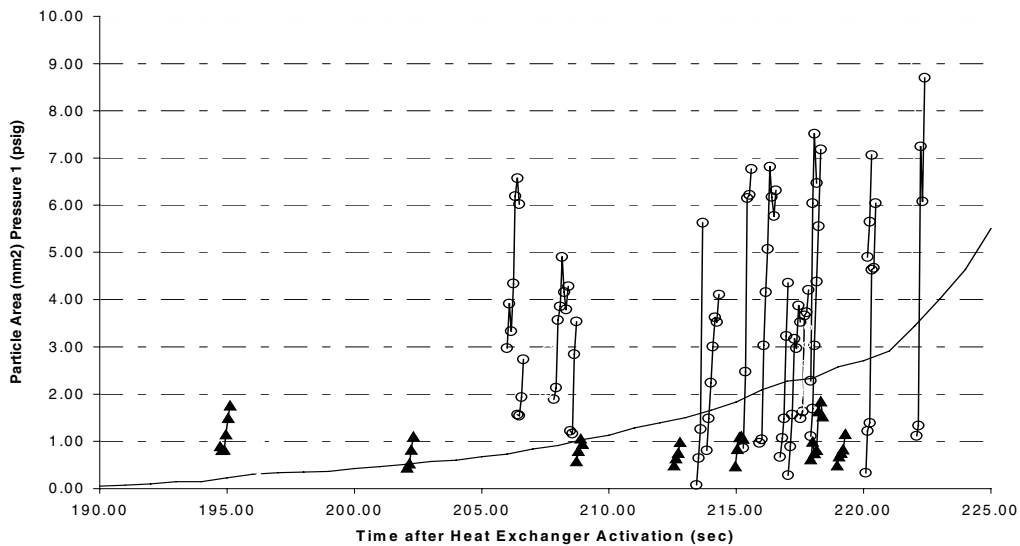


**Fig. 5. Growth of particles as determined from analysis of images such as those in Fig. 3.** The solid and open triangles correspond to the growth of the single particles and agglomerates respectively. The solid line is the pressure.

Large increases in the effective size of the sodium phosphate dodecahydrate particles are observed in increments of less than a second. Growth rates of the two particle types (single and agglomerate) were determined by regressing the calculated elliptical areas against time. Given the difficulty of measuring even smaller particle dimensions, the areas were fit to a linear expression. For the single particles, the rate of area growth was determined as $2.0 \pm 0.49$ mm$^2$/s and did not significantly vary with the duration of the experiment. Agglomerates were found to grow at an average rate of $13.6 \pm 8$ mm$^2$/s.

For agglomerates, there was an overall increase in the growth rate with increasing run time (see Fig. 4). The fact that the growth rate for the single particles was constant over the experimental run implies that the number of particles participating in the formation of the agglomerate increases with time. Lower velocities will result in an increase in time that the particles can interact with one another. In addition, as the velocity decreases, the critical sedimentation velocity is more rapidly approached.

In all images of the single particles, the major axis is aligned with the direction of flow. The lower axial ratios of the agglomerate particles, compared with the single particles, imply that the agglomerates grow in a direction normal to the flow at a higher rate than axially. For the individual particles, the length growth rate was determined as $3 \pm 1.7$ mm/s, while the minor axis was determined to increase at a rate of $0.8 \pm 0.7$ mm/s. For the aggregates these rates were $6.4 \pm 4.5$ mm/s and $3.1 \pm 1.5$ mm/s, respectively.

The higher axial growth rate for the aggregates than for the single particles implies that the coalescence of the elliptical or rod-like particles occurs when the particles are horizontally and vertically displaced from one another. Whereas the growth rate in the length is increased by about a factor of 2, the growth in the width increases by a factor of greater than 3.

The solid line in Fig. 4 corresponds to the measured upstream pressure. Prior to 150 s, this parameter does not increase; thereafter, it begins to rise slowly. This event has been shown to correlate to the formation of single particles and small clusters. The pressure then increases further, and this region corresponds to the predominance of single particles and small aggregates that are forming the bed. Later in time, the particles are forming large agglomerates, which further contribute to the development of the bed. The increase in pressure correlates to the decrease in the calculated velocity. Processes occurring 150 s after the heat exchanger was activated do not strongly depend on local temperature. The temperature within the channel was observed to stay constant and even to increase slightly during the experiment (Fig. 3).

Based on these results, the development of the sodium phosphate dodecahydrate plug was determined to consist of four events: (1) initial growth of single particles of rod-like or ellipsoidal shape, (2) aggregation of the particles into larger structures, followed by sedimentation, (3) further aggregation into still larger structures and increased deposition, and (4) plug formation.

**Additional Flow Loop Experiments**

In the experiments described, the initial velocity was 8 cm/s and the starting flow rate was 3.5 gph. Plug formation was determined to take about 240 s with a cooling water rate for the second heat exchanger at 1.2 gpm. Earlier screening experiments indicated that, at the same cooling water flow rate, increasing the starting velocity to 15 cm/s or a flow rate of 6.8 gph resulted in a time to plug of about 3000 s. Consequently, additional experiments were performed at the higher flow rate to evaluate the effect of velocity on the plug formation process.

Images collected during the experiment were similar to those observed during the low-velocity experiment. The width and length dimensions of the particles were quantified, and growth rates were determined as before. The processes leading to plugging were the same for both experiments. Single crystals formed, followed by aggregates along with the single particles, and finally the dominance of aggregates and complete blockage of the channel.

Experiments as a function of cooling water flow rate and phosphate concentration were also performed. A summary of these data is presented in Table 1.

**Table 1. Growth rates obtained from the runs where image analysis was performed**

| Supernatant flow (gph) | PO$_4$ M | Cooling water flow (gpm) | Time to plug (s) | Temperature at plug (°C) | Particle growth rate (mm$^2$/s) | Agglomerate growth rate (mm$^2$/s) |
|---|---|---|---|---|---|---|
| 3.5 | 0.22 | 1.2 | 230 | 38.6 | 2 ± 0.5 | 14 ± 8 |
| 6.8 | 0.22 | 1.2 | 2950 | 41.8 | 2 ± 0.5 | 19 ± 11 |
| 6.8 | 0.22 | 0.4 | 4207 | 43.2 | 1.5 ± 0.7 | 19 ± 9 |
| 6.8 | 0.15 | 3 | 3790 | 35.9 | 1.6 ± 0.7 | 19 ± 9 |

Reduced growth rates were observed for the experiments at the lower cooling water flow rate and at the lower phosphate concentration of 0.15 *M*. Decreasing the cooling water flow rate from 1.2 to 0.4 gpm for the base composition resulted in a 43% increase in the time needed to form a plug. The time to plug and the heat flux ($q = m\ \rho Cp\Delta T$), for the data obtained at the 0.22 *M* phosphate concentration at the 6.8 gph surrogate flow rate, are linear functions of the final or plug temperature The corresponding expressions allow for the establishment of the initial range where a phosphate plug will form, based on the initial surrogate composition and decrease in temperature. In order to avoid a plug at a supernatant composition of 0.22 *M* phosphate, it is necessary to maintain the temperature of the stream at above 44°C.

**Critical Dimension Determination**

Determination of the critical velocity will depend upon the stream velocity, *V;* the gravitational constant, *g;* a characteristic particle dimension, *W\** (taken here as the width of the particle); the channel diameter, *d*; and the densities ($\rho$ values for the particles and carrier fluid) (Durand 1952)

$$V_{crit} = (V^2/2gW^*)\{2gd((\rho-\rho_t)/\rho_t)\}^{0.5} \ .$$

Figure 6 provides the calculated critical widths and the widths measured during image analysis against the measured velocities. The plot contains data pertinent only to the single particles. Some of the measured particle widths for the lower–flow-rate experiment (3.5 gph) were very close to the calculated critical widths, and the particles were found to be undergoing sedimentation. In contrast, the particle widths determined from the images for the higher-velocity run (6.8 gph) were all smaller than the calculated critical dimensions. Here the development of the moving bed occurred principally through particle agglomeration. The estimated intersection of the measured particle widths with the calculated critical widths was around 9 cm/s. Development of the plug took longer at the higher Reynolds number owing to the larger difference between the initial velocity and the critical velocity.

The measured widths at the initial 15 cm/s velocity were clustered around a 0.5- to 0.7-mm regime. For the data at 6.8 gph, the average width was determined as 0.61 ± 0.12. Lowering the cooling water flow rate yielded a value of 0.57 ± 0.04, while changing the phosphate concentration to 0.15 *M* yielded a mean width of 0.49 ± 0.03 mm. The weak trend in the decrease of the widths with a reduction in the cooling water flow rate and the phosphate concentration is consistent with the reduced single-particle growth rates for these conditions

**Application of Models to Describe the Observed Increase in Pressure and the Effect of Cooling Water Flow Rate**

The data indicate that the particles were behaving similarly at the different flow rates. The growth of the bed was also similar (Lindner et al. 2000). The pressure traces from the different runs, when normalized by the plugging time, were found to be superimposable, indicating the similarity in the particle growth,

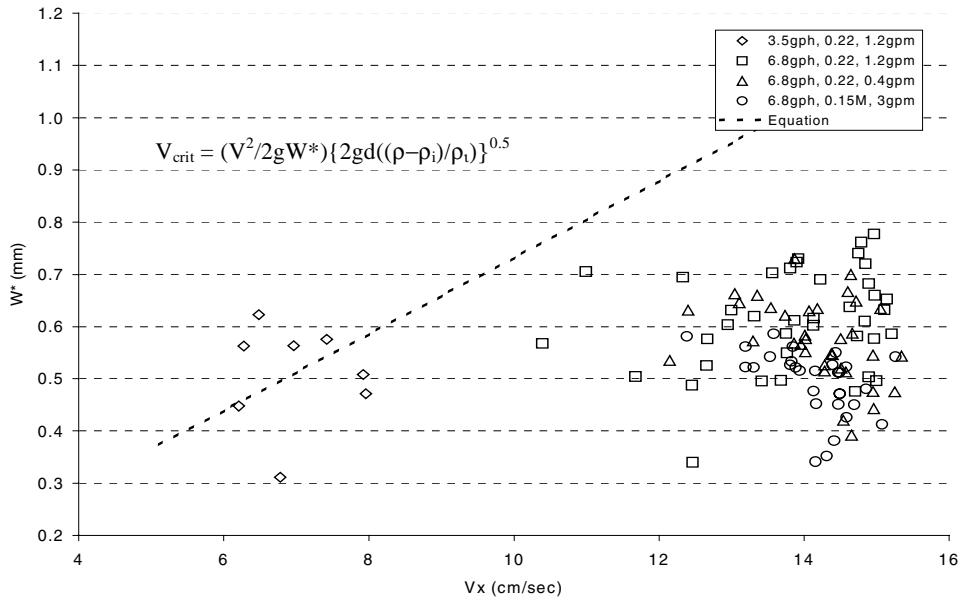$$V_{crit} = (V^2/2gW^*)\{2gd((\rho-\rho_i)/\rho_t)\}^{0.5}$$

**Fig. 6. Measured and calculated critical widths (open and solid symbols) for the experiments at 8 and 15 cm/s with 1.2 gph cooling water flow applied to heat exchanger 2.**

aggregation, and bed formation processes. The temporal delays in plug formation were found to result from the differences between the initial velocities and the calculated critical velocities. The delay at the 6.8 gph flow rate, compared with the 3.5 gph flow rate, is a result of the particles growing to a similar size prior to deposition. The critical velocity is reached later for the higher flow rate.

The pressures were found to be well predicted by the model of Wilson (Wilson 1996; Mason and Levy 2001). This model considers a particle bed comprising dense solids; the liquid is isotropic. The bed area was determined from the collected images, and the liquid fraction was obtained by subtraction. Both the solid and liquid phases are assumed to share a common pressure. As the solid fraction is amassed within the channel, the corresponding pressure increases. Full details of the calculations can be found in Wilson (1996) and Mason and Levy (2001).

In all the experiments, the downstream fluid temperatures show a rapid decrease from the initial 46°C value immediately following activation of the heat exchanger. A gradual decrease is then observed, followed by a near-constant temperature. The thermal profile of the fluid during the experiment corresponds to unsteady convection, and a number of models are available for comparison with the measured temperatures. For example, this work found that the model of Krishan (1982) adequately describes the observed behavior. The formalism accounts for a step change in the heat extracted from the channel and solves the associated energy expressions using term-by–term inversion. Data were then fit and compared with those expressions obtained for the experimental temperatures using the same functional equation form ($T = (T/t)ln(time) + T$). Agreement with the model can be observed in Table 2, where the associated slopes and limiting temperatures are collected. Table 2 also shows the results of experiments at the surrogate flow rate of 6.8 gph at different cooling water flow rates, and an experiment conducted at a surrogate flow of 5 gph with a cooling water flow rate of 1.2 gpm.

The model predictions are within 2% for the limiting temperatures. Somewhat larger errors are observed on comparing the decrease in temperature with time. These values, especially for the experiments at the

**Table 2. Time to plug and results of experimental and model fits of the downstream channel temperature**

| Supernatant flow rate (gph) | HEX2 flow rate (gpm) | Time to plug (s) | Experimental T/t (°C/s) | T (°C) | Model of Krishan (14) | |
|---|---|---|---|---|---|---|
| | | | | | T/t (°C/s) | T (°C) |
| 3.5 | 1.2 | 230 | –1.41 | 38.6 | –1.25 | 39.3 |
| 5.0 | 1.2 | 319 | –1.16 | 40.4 | –0.83 | 40.9 |
| 6.8 | 1.2 | 2950 | –0.85 | 41.8 | –0.74 | 41.6 |
| 6.8 | 0.7 | 3359 | –0.37 | 41.6 | –0.46 | 41.3 |
| 6.8 | 0.6 | 3613 | –0.28 | 42.3 | –0.38 | 42.1 |
| 6.8 | 0.4 | 4207 | –0.24 | 43.2 | –0.26 | 43.0 |

higher supernatant flow rates, are influenced by the cycling of the immersion heater within the surrogate holding tank.

**Establishment of an Operating Regime**

The temperatures measured upon plug formation are plotted against the heat flux divided by the mass flow rate in Fig. 7. All of the data for the 0.22 *M* phosphate composition are observed to fall on a straight line. Additional experiments were performed with the original constituents in the base composition but lowering the phosphate concentration to 0.15 and 0.11 *M*.
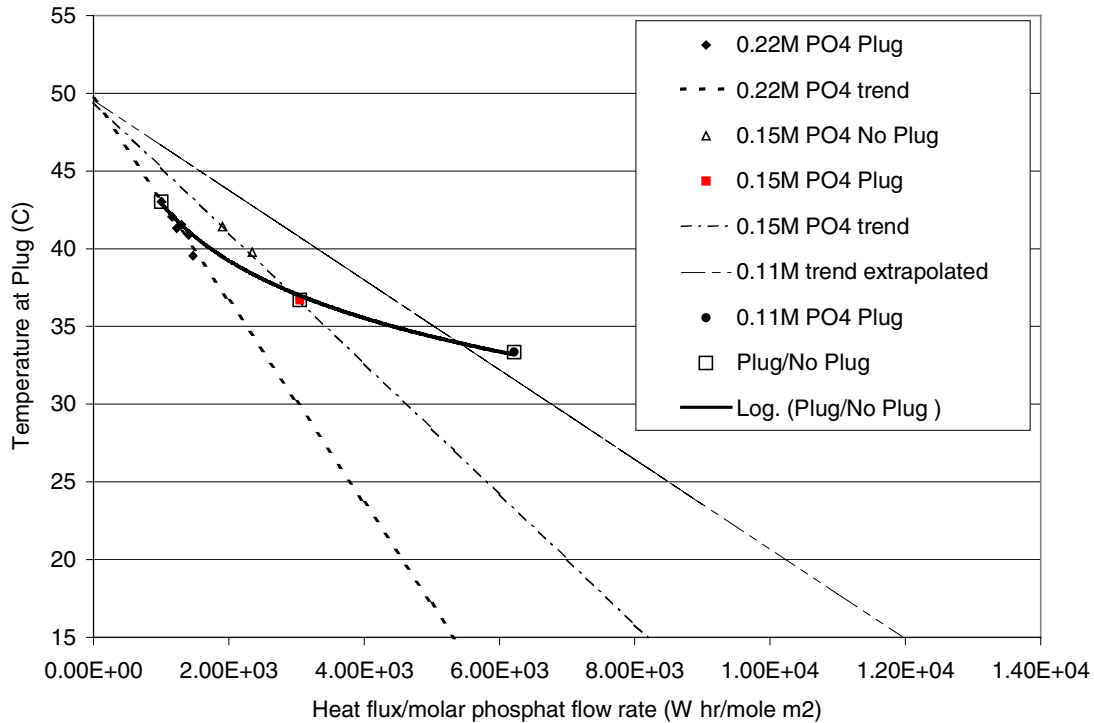


**Fig. 7. Plot illustrating the relations of the plug temperature with the heat lost by the surrogate solutions.**

The data for the 0.15 *M* phosphate concentration appear to follow a linear relationship, but with a slightly different slope. In an attempt to establish whether a lower-concentration surrogate would form a plug, the slopes from the two data sets were regressed against the phosphate concentration. The dashed lines in Fig. 7 show the resulting expression and the results of the final experiment with a phosphate concentration of 0.11 *M*.

The plug/no plug line denoted as solid in Fig. 7 was obtained by fitting the temperature/reduced heat flux for 0.22 *M* phosphate surrogate at a cooling water flow rate of 0.4 gpm, with the same data for the 0.15 *M* phosphate concentration at 3 gpm and the temperature obtained from the 0.11 *M* phosphate run where two heat exchangers were employed. This demarcation is believed to be the best representation of which temperatures and phosphate concentrations will result in a plug, although some safety margins will be required in actual practice.

Because of practical limitations, the ability to increase the flow velocity of the waste is limited by the rate of infusion of the liquid into the salt well screen. Consequently, the most appropriate action to prevent a plug is to either maintain the temperature above the crystallization point, and/or dilute the waste so that, should the temperature of the fluid decrease radically, particles will not form. Determination of the average phosphate concentration in the actual supernatant stream will allow for an assessment of how large a dilution factor is needed based on the heat tracing for a given route.

**6.4 Conclusions**

Salt well pumping flow-loop experiments were conducted on a surrogate composition for Hanford tank 241-SX-104 as a function of solution flow rate, cooling water flow, and phosphate concentration. Particle dimensions and growth rates were determined from analysis of images of the stream collected when a portion of the channel was replaced with a clear Plexiglass pipe. Single-particle growth rates were determined for the baseline composition as a function of cooling water flow rate. The maximum value was found to be $2 \pm 0.5$ mm$^2$/s. Agglomerates were observed with growth rates of as high as 19 mm$^2$/s. Plug formation was determined to result from sedimentation of sufficiently large single particles and agglomerates, followed by the development of a moving bed flow. Experiments were continued until complete blockage of the channel occurred.

A two-phase flow model originally developed by Wilson (1996) was found to agree with the increase of pressure as plug formation proceeded. The process was characterized by unsteady convective flow, which was found to be well represented by the framework advanced by Krishan (1982). Experiments performed at different phosphate concentrations and at different heat exchanger cooling rates were used to construct an operating envelope that related the temperature upon plug formation to the ratio of the heat flux over the phosphate concentration.

**6.5 References**

Durand, R., 1952. *The Hydraulic Transportation of Coal and Other Materials in Pipes*, Colloquium, National Coal Board, London.

Fluor Daniel Hanford 1998. *Single-Shell Tank Retrieval Program Mission Analysis Report*, Fluor Daniel Hanford, Richland, Washington.

Herting, D. L., 1998. *Tank 241-SX-104 Dilution Testing, Interim Report*, Internal Memo 8C510-PC98-024, Numatec Hanford Corporation, Richland, Washington.

Hunt, R. 2000. Personal communication to J. S. Lindner, Mississippi State University, Starkville, Mississippi.

Krishan, B. 1982. "On Conjugated Heat Transfer in Fully Developed Flows," *Int. J. Heat Mass transfer*, **25**, p. 288.

Lindner, J. S., et al. 2000. *Transport Studies on Interim Stabilization Supernatant Streams, FY 2000 Progress Report*, Diagnostic Instrumentation and Analysis Laboratory, Mississippi State University, Starkville, Mississippi (October).

Lindner, J. S., Al Habbash, H., and R. K. Toghiani 2000. "Prevention of Solids Formation" in *DIAL Quarterly Report,* DE-FC26-98FT40395-9, Diagnostic Instrumentation and Analysis Laboratory, Mississippi State University, Starkville, Mississippi.

Mason, D. J., and A. Levy 2001. "A Model for Non-Suspension Gas-Solids Flow of Fine Powders in Pipes," *Intl J. Multiphase Flow*, **27**, pp. 415–435.

Reynolds, D. A., 2000. "Status of Waste Transfers, Criteria, and Plans," presented at the Third Saltcake Dissolution and Feed Stability Workshop, Richland Washington, May 16, 2000.

Steen, F. H., 1999. *Ammonia Analysis Results for the Final Report for Tank 241-SX-104*, Memo WMH-9852843, Numatec Hanford Corporation, Richland, Washington.

Wilson, K. C., et al., 1996. *Hydraulic Conveying of Solids with Centrifugal Pumps*, Chapman and Hall, London.

**Acknowledgement**

## INTERNAL DISTRIBUTION

| | | | |
|---|---|---|---|
| 1. | J. M. Begovich | 10. | S. M. Robinson |
| 2. | V. F. de Almeida | 11. | C. Tsouris |
| 3. | D. W. Depaoli | 12. | J. S. Watson |
| 4. | R. D. Hunt | 13. | C. F. Weber |
| 5. | J. N. Herndon | 14–19. | T. D. Welch |
| 6. | R. T. Jubin | 20. | ORNL Laboratory Records–OSTI |
| 7. | B. E. Lewis | 21. | ORNL Laboratory Records–RC |
| 8. | C. P. McGinnis | 22. | Central Research Library |
| 9. | D. A. Palmer | | |

## EXTERNAL DISTRIBUTION

23. H. Alhabbash, Diagnostic Instrumentation and Analysis Laboratory, 205 Research Boulevard, Starkville, MS 39759-9734
24. D. Baide, CH2M Hill Hanford Group, P.O. Box 1500, MSIN S7-90, Richland, WA 99352
25. B. Barton, CH2M Hill Hanford Group, P.O. Box 1500, MSIN R-11, Richland, WA 99352
26. J. Bell, 137 Bowsprit Lane, Kingston, TN 37763
27. B. Brendel, CH2M Hill Hanford Group, P.O. Box 1500, MSIN S7-90, Richland, WA 99352
28. J. Bryant, Pacific Northwest National Laboratory, P.O. Box 999, MSIN K7-94, Richland, WA 99352
29. W. Callaway, Cogema Engineering Corporation, P.O. Box 1000, MSIN T6-07, Richland, WA 99352
30. J. Cammann, CH2M Hill Hanford Group, P.O. Box 1500, MSIN T4-08, Richland, WA 99352
31. B. Carteret, Pacific Northwest National Laboratory, P.O. Box 999, MSIN K9-91, Richland, WA 99352
32. A. B. Carlson, Numatec Hanford Corporation, P.O. Box 1300, MSIN R3-73, Richland, WA 99352
33. A. F. Choho, Numatec Hanford Corporation, , P.O. Box 1300, MSIN H6-22, Richland, WA 99352
34. D. Crass, Numatec Hanford Corporation, P.O. Box 1300, MSIN S7-90, Richland, WA 99352
35. J. Cruz, Department of Energy, Office of River Protection, P.O. Box 550, MSIN H6-60, Richland, WA 99352
36. R. Edwards, Westinghouse Savannah River Company, Building 704-3N, Aiken, SC 29808
37. F. F. Erion, Pacific Northwest National Laboratory, P.O. Box 999, MSIN K7-15, Richland, WA 99352
38. S. Estey, CH2M Hill Hanford Group, P.O. Box 1500, MSIN R2-11, Richland, WA 99352
39. A. Felmy, Pacific Northwest National Laboratory, P.O. Box 999, MSIN K8-96, Richland, WA 99352
40. K. Gasper, CH2M Hill Hanford Group, P.O. Box 1500, MSIN L4-07, Richland, WA 99352
41. P. Gauglitz, Pacific Northwest National Laboratory, P.O. Box 999, MSIN K6-28, Richland, WA 99352
42. D. Geniesse, Cogema Engineering Corporation, 2425 Stevens Drive, Richland, WA 99352
43. P. Gibbons, Numatec Hanford Corporation, P.O. Box 1300, MSIN K9-91, Richland, WA 99352
44. R. Gilchrist, Pacific Northwest National Laboratory, P.O. Box 999, MSIN K9-91, Richland, WA 99352
45. J. Henshaw, AEA Technology, B220 Harwell, Didcot, Oxfordshire, UK, OX11 0QJ
46. D. Herting, Fluor Hanford, P.O. Box 1000, MSIN T6-07, Richland, WA 99352
47. J. Honeyman, CH2M Hill Hanford Group, P.O. Box 1500, MSIN H6-18, Richland, WA 99352
48. J. Huckaby, Pacific Northwest National Laboratory, P.O. Box 999, MSIN K7-15, Richland, WA 99352
49. J. Jewett, Numatec Hanford Company, P.O. Box 1300, MSIN R3-73, Richland, WA 99352

50. G. Josephson, Pacific Northwest National Laboratory, P.O. Box 999, MSIN K6-69, Richland, WA 99352
51. L. J. Julyk, CH2M Hill Hanford Group, P.O. Box, 1500, MSIN R3-83, Richland, WA 99352
52. N. W. Kirch, CH2M Hill Hanford Group, P.O. Box, 1500, MSIN R3-73, Richland, WA 99352
53. R. Kirkbride, Numatec Hanford Company, P.O. Box 1300, MSIN R3-73, Richland, WA 99352
54. W. L. Kuhn, Pacific Northwest National Laboratory, P.O. Box 999, MSIN K7-15, Richland, WA 99352
55. J. Lindner, Diagnostic Instrumentation and Analysis Laboratory, 205 Research Boulevard, Starkville, MS 39759-9734
56. R. López, Florida International University, 10555 West Flagler St., CEAS 2100, Miami, FL 33174
57. R. Luyendijk, Waste Policy Institute, 2000 Craft Drive, Suite 1000, Blacksburg, VA 24060
58. G. MacLean, Fluor Federal Services, P.O. Box 1050, MSIN G3-10, Richland, WA 99352
59. B. Mauss, Department of Energy, Office of River Protection, P.O. Box 550, MSIN H6-60, Richland, WA 99352
60. P. Meyer, Pacific Northwest National Laboratory, P.O. Box 999, MSIN K7-15, Richland, WA 99352
61. J. Morin, Westinghouse Savannah River Co., 703-H Bldg./Rm. 119 Aiken, SC 29808
62. J. Noble-Dial, U.S. Department of Energy, Oak Ridge Operations Office, 55 Jefferson, Oak Ridge, TN 37831
63. Y. Onishi, Pacific Northwest National Laboratory, P.O. Box 999, MSIN K7-15, Richland, WA 99352
64. R. Orme, Numatec Hanford Company, P.O. Box 1300, MSIN R3-73, Richland, WA 99352
65. J. Pike, Westinghouse Savannah River Co., Building 704-196N, Aiken, SC 29808
66. J. Plodinec, Diagnostic Instrumentation and Analysis Laboratory, 205 Research Boulevard, Starkville, MS 39759-9734
67. M. Poirier, Westinghouse Savannah River Company, Building 773-42A, Aiken, SC 29808
68. D. Reynolds, CH2MHill Hanford Group, Inc., MSIN: R2-11, 2440 Stevens Center, P.O. Box 1500, Richland, WA 99352-1505
69. J. Roecker, 17123 North Brookside Lane, Colbert, WA 99005
70. W. Schulz, W2S Company, 12704 Sandia Ridge Place, NE, Albuquerque, NM 87111
71. R. Srivastava, Florida International University, 10555 West Flagler Street, CEAS 2100, Miami, FL 33174
72. Tanks Focus Area Headquarters Program Lead, c/o Kurt Gerdes, DOE Office of Science and Technology, 19901 Germantown Road, 1154 Cloverleaf Building, Germantown, MD 20874-1290
73. Tanks Focus Area Program Manager, c/o T. P. Pietrok, U.S. Department of Energy, Richland Operations Office, P.O. Box 550, MSIN K8-50, Richland, WA 99352
74. Tanks Focus Area Technical Team, c/o B. J. Williams, Pacific Northwest National Laboratory, P.O. Box 999, MSIN K9-69, Richland, WA 99352
75. L. Tavlarides, Syracuse University, Dept. of Chemical Engineering & Materials Science, 334 Hinds Hall, Syracuse, NY 13244-1190
76. J. Thompson, Department of Energy, Office of River Protection, P.O. Box 550, MSIN H6-60, Richland, WA 99352
77. M. Thompson, Westinghouse Savannah River Company, Savannah River, Technology Center Building, 773-A, C140 Aiken, SC 29802
78. R. Thompson, CH2M Hill Hanford Group, P.O. Box 1500, MSIN T4-08, Richland, WA 99352
79. R. Toghiani, Mississippi State University, School of Chemical Engineering, P.O. Box 9595, MS State, MS 39762
80. G. Vandegrift, Argonne National Laboratory, Building 205, 9700 South Cass Avenue, Argonne, IL 60439
81. D. T. Vladimirof, CH2M Hill Hanford Group, P.O. Box 1500, MSIN S7-20, Richland, WA 99352
82. F. Washburn, Westinghouse Savannah River Company, Building 704-196N, Aiken, SC 29808
83. T. Weber, 6622 West Victoria Avenue, Kennewick, WA 99336
84. J. Westsik Jr., Pacific Northwest National Laboratory, P.O. Box 999, MSIN K9-91, Richland, WA 99352